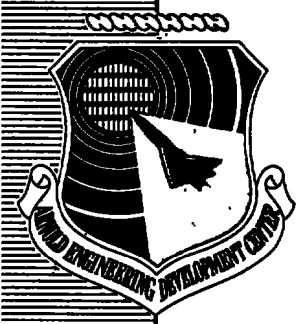

DESIGN AND EVALUATION OF A LASER DOPPLER VELOCIMETER FOR THE AEDC-PWT 4-FT TRANSONIC TUNNEL

F. L. Crosswy and D. B. Brayton
ARO, Inc., A Sverdrup Corporation Company

PROPULSION WIND TUNNEL FACILITY
ARNOLD ENGINEERING DEVELOPMENT CENTER
AIR FORCE SYSTEMS COMMAND
ARNOLD AIR FORCE STATION, TENNESSEE 37389

July 1978

Final Report for Period July 1976 - October 1977

Prepared for

ARNOLD ENGINEERING DEVELOPMENT CENTER/DOTR
ARNOLD AIR FORCE STATION, TENNESSEE 37389

NOTICES
When U. S. Government drawings, specifications, or other data are used for any purpose other than a definitely related Government procurement operation, the Government thereby incurs no responsibility nor any obligation whatsoever, and the fact that the Government may have formulated, furnished, or in any way supplied the said drawings, specifications, or other data, is not to be regarded by implication or otherwise, or in any manner licensing the holder or any other person or corporation, or conveying any rights or permission to manufacture, use, or sell any patented invention that may in any way be related thereto.
Qualified users may obtain copies of this report from the Defense Documentation Center.
References to named commerical products in this report are not to be considered in any sense as an indorsement of the product by the United States Air Force or the Government.

This report has been reviewed by the Information Office (OI) and is releasable to the National Technical Information Service (NTIS). At NTIS, it will be available to the general public, including foreign nations.

APPROVAL STATEMENT

This report has been reviewed and approved.

Marshall K. Kingery

MARSHALL K. KINGERY
Project Manager, Research Division
Directorate of Test Engineering

Approved for publication:

FOR THE COMMANDER

Marion L. Laster

MARION L. LASTER
Director of Test Engineering
Deputy for Operations

REPORT DOCUMENTATION PAGE		READ INSTRUCTIONS BEFORE COMPLETING FORM
1 REPORT NUMBER AEDC-TR-78-30	2. GOVT ACCESSION NO.	3 RECIPIENT'S CATALOG NUMBER
4 TITLE (and Subtitle) DESIGN AND EVALUATION OF A LASER DOPPLER VELOCIMETER FOR THE AEDC-PWT 4-FT TRANSONIC TUNNEL		5 TYPE OF REPORT & PERIOD COVERED Final Report, July 1976-October 1977 6. PERFORMING ORG. REPORT NUMBER
7 AUTHOR(s) F. L. Crosswy and D. B. Brayton ARO, Inc.		8 CONTRACT OR GRANT NUMBER(s)
9 PERFORMING ORGANIZATION NAME AND ADDRESS Arnold Engineering Development Center Air Force Systems Command Arnold Air Force Station, TN 37389		10 PROGRAM ELEMENT, PROJECT TASK AREA & WORK UNIT NUMBERS Program Element 65807F
11. CONTROLLING OFFICE NAME AND ADDRESS Arnold Engineering Development Center (DOS) Arnold Air Force Station, TN 37389		12 REPORT DATE July 1978 13. NUMBER OF PAGES 58
14 MONITORING AGENCY NAME & ADDRESS(if different from Controlling Office)		15. SECURITY CLASS. (of this report) UNCLASSIFIED 15a. DECLASSIFICATION/DOWNGRADING SCHEDULE N/A

16 DISTRIBUTION STATEMENT (of this Report)
Approved for public release; distribution unlimited.

17 DISTRIBUTION STATEMENT (of the abstract entered in Block 20, if different from Report)

18 SUPPLEMENTARY NOTES
Available in DDC.

19 KEY WORDS (Continue on reverse side if necessary and identify by block number)
laser Doppler velocimeters
flow angle measurements
velocity measurements

20. ABSTRACT (Continue on reverse side if necessary and identify by block number)
The design details and initial performance evaluation of a two-component Laser Doppler Velocimeter (LDV) system for a large transonic wind tunnel are presented. The two-color, backscatter LDV was specially developed for free-stream, pitch plane flow angle and velocity magnitude measurements using only intrinsic particulate matter as light scatterers. An environmental control system and remote optical alignment techniques were developed

DD FORM 1 JAN 73 1473 EDITION OF 1 NOV 65 IS OBSOLETE

20. ABSTRACT (Continued)

since the LDV was located in the hostile environment (vibration, vacuum, inaccessibility, etc.) of the tunnel plenum region. A new-type LDV signal processor was developed to process the low-level signals produced by the small intrinsic particles. A versatile, computer-based system was developed for high-speed data acquisition. LDV mean velocity and flow angle data are compared to free-stream velocity data and aerodynamic flow angle probe data.

AFSC
Arnold AFS Tenn

PREFACE

The work reported herein was conducted by the Arnold Engineering Development Center (AEDC), Air Force Systems Command (AFSC), under Program Element 65807F. The results of the research were obtained by ARO, Inc., AEDC Division (a Sverdrup Corporation Company), operating contractor for the AEDC, AFSC, Arnold Air Force Station, Tennessee, under ARO Project Numbers P32S-C0A and P32I-K1A. The manuscript was submitted for publication on April 13, 1978.

The authors wish to acknowledge the contributions of H. T. Kalb and J. H. Brewer, ARO, Inc., who wrote Sections 3.4 and 3.6, respectively.

CONTENTS

Page

1.0 INTRODUCTION 5
2.0 DESIGN CONSTRAINTS
2.1 AEDC-PWT Transonic Tunnel 4T 6
2.2 Design Considerations 7
3.0 VELOCIMETER SYSTEM DESCRIPTION
3.1 Environmental Control System 9
3.2 Single-Velocity-Component LDV Optics 11
3.3 Two-Velocity-Component LDV 13
3.4 LDV Signal Processors 18
3.5 Instrumentation and Controls 22
3.6 Data Acquisition Systems 24
4.0 PROCEDURES
4.1 Calibration 25
4.2 Data Reduction 29
4.3 Measurement Uncertainties 32
5.0 TEST RESULTS
5.1 Single-Velocity-Component Measurements 39
5.2 Two-Velocity-Component and Flow Angle Measurements 44
6.0 SUMMARY OF RESULTS AND CONCLUSIONS 51
REFERENCES 53

ILLUSTRATIONS

Figure

1. Aerial View of the Propulsion Wind Tunnel Facility 6
2. Tunnel 4T General Arrangement 7
3. Laser Doppler Velocimeter Installation in Tunnel 4T 10
4. Details of 4T ECS Assembly 11
5. Two-Color LDV Optics Mounted in the ECS 12
6. Single-Velocity-Component LDV Optics 13
7. Two-Color LDV Optics 14
8. Details of the LDV/ECS Assembly 16
9. Doppler Data Analyzer 20
10. Block Diagram of Computer-Based Data Acquisition System, Electronic Instrumentation, and Controls 22
11. Block Diagram of Minicomputer System 24

Figure Page

12. Geometric Determination of LDV Calibration Factor 26
13. Apparatus for Photographing the LDV Fringe Pattern with Vertical Reference Line 27
14. Photographic Determination of Fringe Orientation Angle 28
15. Geometric Relationship of Velocity Vector $\overline{V}_i$ and LDV Measurement Axes 31
16. Uncertainty in the Measurement of a Single Velocity Component 36
17. LDV Signal Characteristics: Particle Size and Number Density Effects 40
18. Signal Waveform at Mach Number 1.6 with H_2O Condensate 42
19. Single-Velocity-Component Measurements at the Tunnel Centerline 44
20. Apparatus Details: Flow Angularity Survey in Tunnel 4T 45
21. Sensitivity of x-z Plane Flow Angle to x-Axis Position at Mach Number 0.8 46
22. LDV Measurement Repeatability Test at Mach Number 0.8 47
23. Effect of Trigger Setting (Particle Size) on LDV Measurement Repeatability at Mach Number 0.8 48
24. Scan of y-Axis: x-z Plane Flow Angle and Velocity Magnitude Measurements at Mach Number 0.8 49
25. Scan of y-Axis: x-z Plane Flow Angle and Velocity Magnitude Measurements at Mach Number 0.4 50
26. LDV Data with H_2O Condensate Purposely Formed at Mach Number 0.8 51

TABLES

1. LDV Window Characteristics 17
2. Uncertainty Parameters: Single-Velocity Component Velocity Measurements 35
3. Uncertainty Parameters: Two-Velocity-Component Measurements 37
4. Uncertainty Parameters: Flow Angle Measurements 38
5. 4T LDV Data Productivity Summary 43

NOMENCLATURE 56

1.0 INTRODUCTION

Velocity magnitude and flow angle in the test section of a wind tunnel are two parameters of particular interest in aerodynamic testing. Generally speaking, a spatial distribution of flow angles will exist in the vicinity of a test article. The integration of differential flow-angle-induced forces by the surfaces of the model produces resultant forces and moments which may obscure true aerodynamic characteristics of the test article. Frequently a model will be tested and then returned, with modifications, for further testing. It is essential, therefore, in obtaining basic aerodynamic model performance data or in assessing the effect of modifications to a model that flow angularity effects be accounted for.

Flow angularity in the 4-ft Transonic Wind Tunnel (4T) at AEDC has been the subject of several flow angle probe studies. It has been found that flow angles are affected by such controlled factors as wall porosity and diffuser flap position, as well as by uncontrolled perturbations due to such diverse factors as dust contamination of the stilling chamber smoothing screens or nonuniform alignment of stilling chamber honeycomb panels. The use of mechanical probes to continuously monitor variations in tunnel flow angularity during model tests in 4T is not practical since the probe is normally mounted on the model sting support. Therefore, even though tunnel empty flow angle versus tunnel condition information is available, there is still some uncertainty as to test section flow angle characteristics during model tests.

During the past decade several advances in nonintrusive electro-optical instrumentation systems have occurred which indicate that noninterfering, continuous monitoring of the flow in a tunnel such as 4T is feasible. For example, Laser Doppler Velocimetry, which exploits the Doppler shift of scattered laser radiation for the measurement of microscopic particle velocities, has been used to measure velocities ranging from 10^{-5} to more than 10^{3} m/sec. Since no material part of a Laser Doppler Velocimeter (LDV) interacts with the flow, the phenomena being studied are undisturbed by the instrument, thus making laser velocimetry valuable in many areas of fluid dynamic research. Moreover, the LDV has been applied successfully in hostile thermal and impact environments where its material probe counterparts could not readily be used. Examples of such applications are velocity measurements in furnace flame investigations (Ref. 1), in a diesel engine combustion chamber (Ref. 2), in solid propellant rocket plumes (Ref. 3), in jet engine exhaust plumes (Ref. 4), and in the interblade regions of jet engine compressors (Ref. 5). Since the LDV does not perturb the fluid flow and is characterized by a small sensing volume, a two-velocity-component system has been used for boundary-layer profile measurements (Refs. 6 and 7) and for measurements across a bow shock (Refs. 8 and 9).

The purpose of this report is (1) to describe the development of an LDV suitable for accurate measurement of free-stream velocity magnitude and flow angle in a large aerodynamic test facility and (2) to evaluate the LDV performance in tests conducted in Tunnel 4T.

2.0 DESIGN CONSTRAINTS

The development of an LDV system capable of operation within Tunnel 4T required numerous design innovations and compromises due to the many environmental constraints imposed by the wind tunnel. The considerations that led to the final design are reviewed herein as a prelude to understanding the final system configuration; the problems that were faced are similar to those that may be encountered in many large aerodynamic test facilities.

2.1 AEDC-PWT TRANSONIC TUNNEL 4T

The 4-ft Transonic Wind Tunnel (4T) of the AEDC Propulsion Wind Tunnel Facility is shown in Fig. 1. Details of the test section segment of the tunnel are shown in

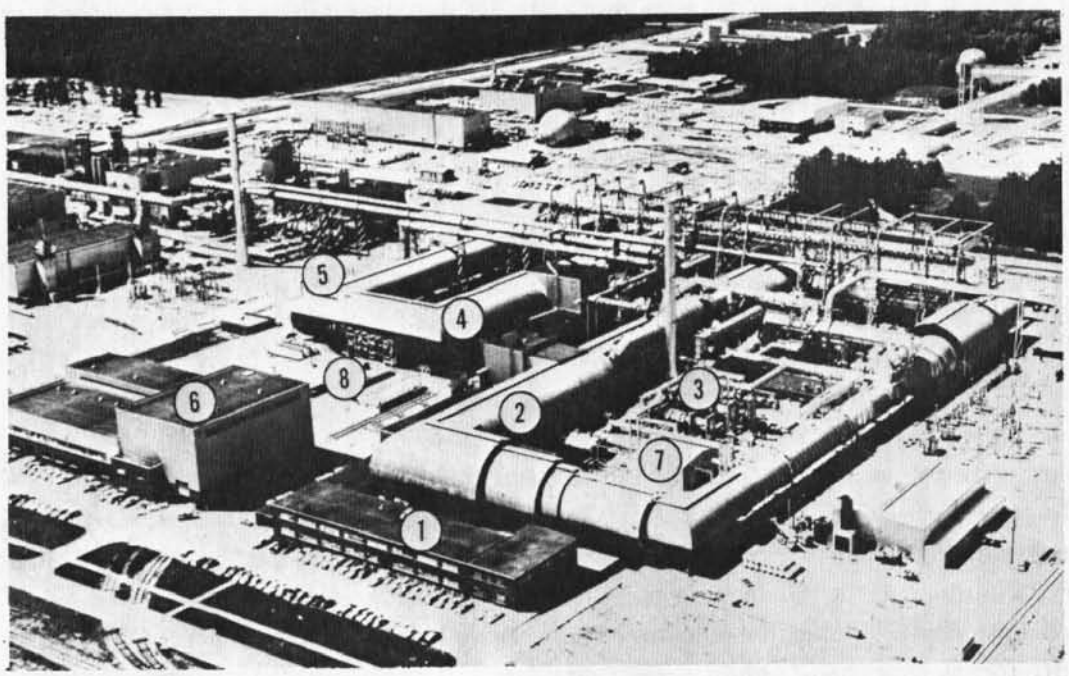

1. Office Building
2. 16-ft Supersonic Tunnel
3. Plenum Evacuation System
4. 16-ft Transonic Tunnel
5. Atmospheric Drier Building
6. Model Installation Building
7. 4-ft Transonic Tunnel
8. Cryogenics System

Figure 1. Aerial view of the Propulsion Wind Tunnel Facility.

Fig. 2. The tunnel is a continuous flow, closed-circuit, variable density, transonic wind tunnel with a test section 4 ft square (cross section) by 12.5 ft long. The basic Mach number range is 0.1 to 1.3. Two separate sets of nozzle block inserts can be installed to provide Mach number 1.6 or 2.0 operation. Variable porosity walls are employed for reduction of wall interference effects. The tunnel stagnation pressure can be varied from 160 to 3,700 psfa, and the stagnation temperature can be controlled to a limited extent over the range from 80 to 160°F (Ref. 10).

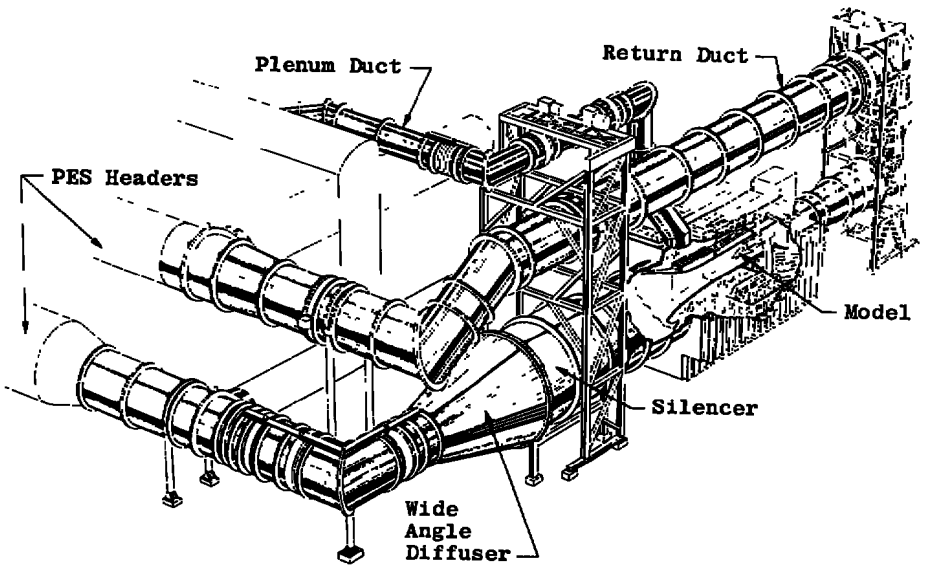

Figure 2. Tunnel 4T general arrangement.

In addition to the conventional sting-mounted force and pressure tests of aerodynamic models, Tunnel 4T can be used for highly specialized testing techniques such as captive-trajectory store separation, store drop studies, magnus effects testing, and dynamic stability investigations.

2.2 DESIGN CONSIDERATIONS

For successful utilization of an LDV the flow being studied must contain particulate matter large enough to scatter sufficient light for signal detection and processing but small enough to respond rapidly to flow transients or accelerations. Furthermore, the concentration of particulates must be high enough that an adequate data rate is obtained but, for the individual realization systems prevalent at AEDC, low enough that only a single particle will be found in the probe volume at any time. Clearly, the most direct approach to these somewhat conflicting requirements is to artificially seed the flow to the desired concentration with particles of a known size. However, the variety and scope of tests performed in 4T is such that artificial seeding is not desirable from a tunnel

operations standpoint and could not be justified in the evaluation of a prototype LDV system.

In many applications, the use of intrinsic particulates does not prove to be especially restrictive to successful LDV utilization since the concentration of particles in the atmosphere is high (10^9 particles/m^3 for diameters $> 0.1\mu m$, Ref. 11). In 4T, however, a tortuous path, viscous filter is used to restrict the passage of particles through the test section. Furthermore, since condensation processes can alter the thermodynamic properties of the working gas in transonic and supersonic flows, the air entering the circuit is dried to limit its moisture content. Although no quantitative data on particle size, number density, or light-scattering characteristics were available for the tunnel, it was expected from the above considerations that the particles present would be small. It was necessary, therefore, to use a high power laser in conjunction with a large collector lens to maximize the probability of detecting small particles.

The 4T test section has porous walls which provide boundary-layer control and aid in shock cancellation to minimize wall interference effects. Accordingly, a plenum chamber surrounds the test section to isolate the flow from ambient conditions. To simplify optical access to the test section it was desirable to locate the LDV inside the tunnel plenum. Since pressures and temperatures within the plenum approach tunnel stagnation conditions, it was necessary that the LDV be provided with an environmental control system (ECS) to prevent electrical breakdown of the photomultiplier tube (PMT) and laser at low pressures and to protect certain critical optical components from temperature extremes. High vibration levels were also known to exist in the plenum area, and thus vibration isolation of the ECS/LDV was required. Such factors significantly complicate LDV operation because the system is obviously not accessible for optical alignment or other adjustments once tunnel operation begins. The development of remote optical alignment and operational techniques was necessary to allow the LDV to be used productively.

Although a large collector lens was desirable, the largest window that could be used at the plenum site was 5 x 6 in. Access to the window was limited, moreover, by the test section wall support structure. Thus the receiver lens diameter was limited to 5 in. or less. The small window restricts the LDV to traversing the flow in a horizontal plane and restricts the design to a coaxial transmitter-receiver, backscatter configuration. Such a system is highly vulnerable to light scattering and reflection from the test section window, thus further reducing the instrument's capability to detect small particles.

Finally, personnel traffic through the plenum area and within the tunnel during model installation and instrumentation checkout (1) required the system to be compact and (2) necessitated the introduction of stringent safety procedures due to the use of a high power laser.

In view of these considerations, the overall 4T LDV effort consisted of a hardware design and development phase followed by a series of tunnel tests to evaluate LDV performance. To achieve the project objectives, several supporting studies and developments were conducted and will be discussed in the remainder of this report. These include:

I. System Developments
   1. Environmental Control System
   2. Two-Color, Two-Velocity-Component LDV Optics
   3. Remote Optical Alignment Devices
   4. Low-Level Signal Processor
   5. Computer-Controlled Data Acquisition System

II. Evaluation Study
   1. Definition of 4T Environmental Constraints
   2. Determination of Ultimate LDV Utility Within Constraints
      a. Data Rate for Unseeded Flow
      b. Measurement Uncertainty

3.0 VELOCIMETER SYSTEM DESCRIPTION

The 4T LDV system consists of 1) an Argon Ion Laser, 2) transmitter-receiver optics, 3) electronics and electrical subsystems, 4) associated mechanical components, 5) Doppler Data Processors (DDP's), and 6) a data acquisition system (DAS). Due to the environmental constraints discussed in Section 2, the 4T LDV was also provided with an environmental control system (ECS). Initially, a single velocity component system was used 1) to verify that adequate particulates were present, 2) to ensure that the various protection and control measures were satisfactory, and 3) to develop adequate operational procedures for the system. Subsequently, a two-velocity-component system which employed two high illuminating power wavelengths of the argon laser was developed for obtaining flow angularity measurements. An overall view of the system developed for 4T is shown in Fig. 3.

3.1 ENVIRONMENTAL CONTROL SYSTEM

The ECS enclosure, shown in Fig. 4, is divided into a laser compartment which is passively pressurized by venting to the atmosphere and an optics compartment which assumes plenum pressure. A connector panel, shown in Fig. 5, is used to connect the

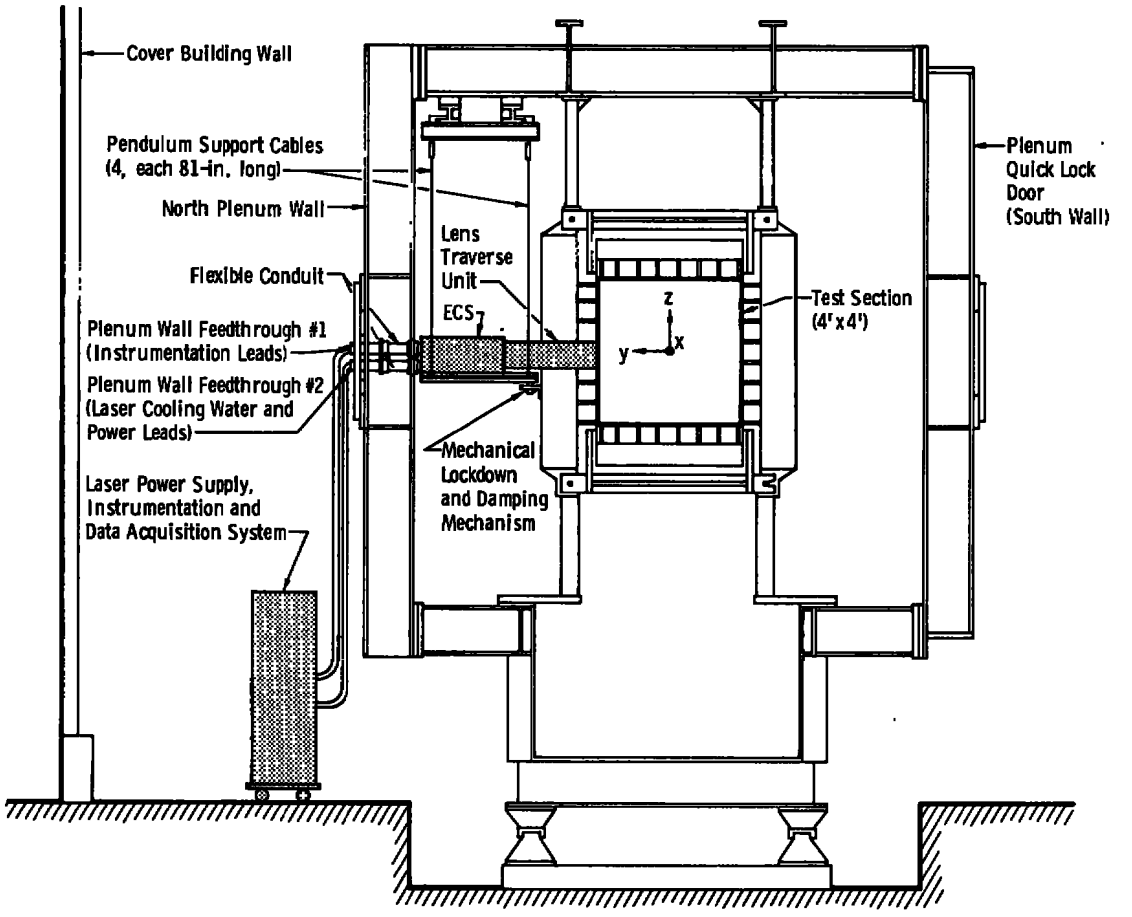

Figure 3. Laser Doppler Velocimeter installation in Tunnel 4T.

instrumentation leads from one compartment to the other. Several gas connectors are also mounted on this panel and are used to connect the PMT housings to the laser compartment to maintain the PMT's at atmospheric pressure. Temperature-sensitive LDV components are mounted on temperature-controlled platens inside the ECS enclosure.

The ECS is completely enclosed so that the LDV optical elements are protected from dust and inadvertant misalignment by personnel working nearby. The spatial orientation of the ECS enclosure with respect to the coordinate system of Fig. 3 is adjusted with six degrees of freedom by use of jackscrew assemblies.

Vibration protection is achieved by suspending the ECS as a pendulum as shown in Fig. 3. The laser cooling water, power leads, and instrumentation cables are fed through flexible conduit to maintain good vibration isolation between the pendulum-mounted ECS and the plenum wall. The natural frequencies in the x-, y-, and z-directions were

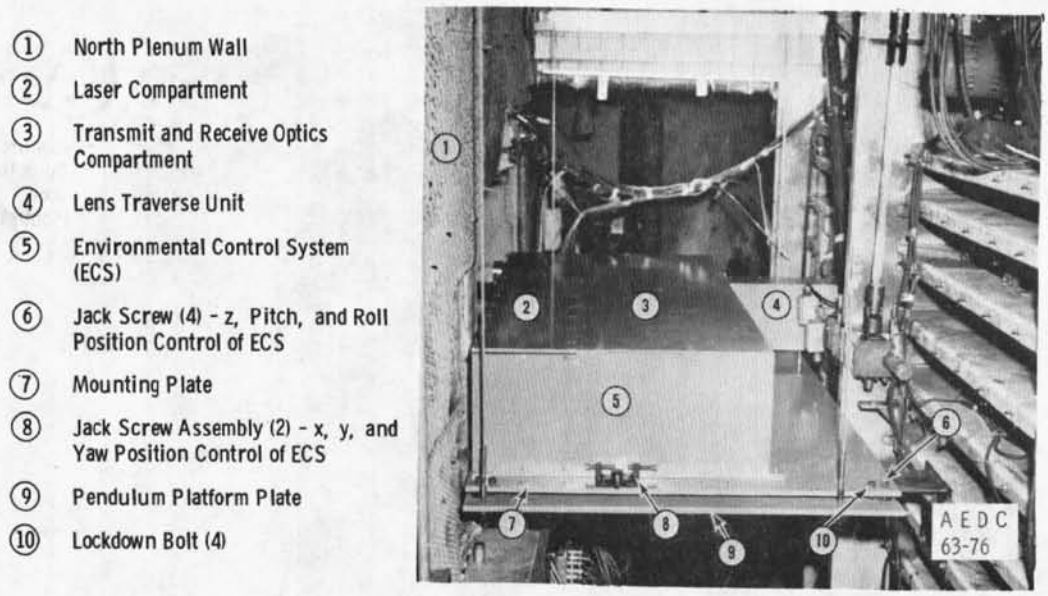

Figure 4. Details of 4T ECS assembly.

found to be 1, 0.7, and 10.5 Hz, respectively. Initial operation of the 4T LDV system showed that the x- and y-axis vibration protection was adequate but that low-level z-axis vibratory forces were still being transmitted through the four support cables. Subjecting the LDV optical elements to these low-level vibrations for extended periods of time (several hours) invariably caused gross optical misalignment. This problem was solved by devising mechanical lockdown devices for the optical elements.

3.2 SINGLE-VELOCITY-COMPONENT LDV OPTICS

The optical schematic for the single-component LDV is shown in Fig. 6. Light from an Argon Ion Laser operating at a 488.0-nm wavelength is directed by mirror M1 to pass through window W1, which separates the pressurized and unpressurized ECS compartments. The lens combination L1 and L2 expands the beam, which is redirected by mirror M2 to a set of optical-path-length-compensated beam splitters, BS1 and BS2. The parallel beams emerging from BS2 enter baffle tube, BT, which provides photon isolation of the transmitter and receiver, and are directed by mirror M3 to pass through the transmitter-receiver lens, L3, which focuses the beams at a point in the test section to form the probe volume, PV. This element was a 5-in.-diam achromatic lens with a nominal primary focal length of 25 in. The maximum diameter of lens L3 was dictated by the restricted mechanical access discussed in Section 2.3. The lens combinations used in the input optics of the one-component LDV formed a probe volume with a 10-mm length and a maximum diameter of 0.2 mm. The fringes formed in the probe volume had a nominal spacing of 12 μm between adjacent intensity maxima.

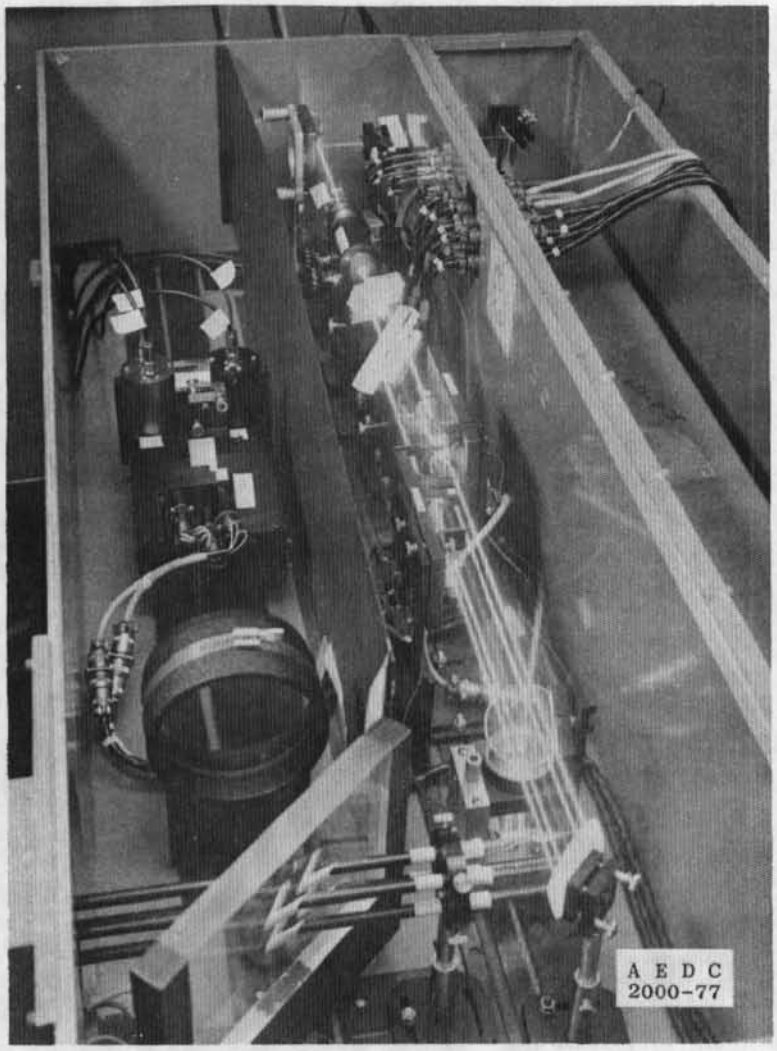

Figure 5. Two-color LDV optics mounted in the ECS.

Light scattered in the back direction by small particles passing through the probe volume is collected and collimated by lens L3. Mirror M4 reflects the collimated light onto lens L4, which is identical to L3. The collected radiation is then focused onto a 200-μm-diam aperture, AP. A laser line filter, LLF, was used to exclude background light, introduced by test section illumination lamps, from the 931A PMT used for signal detection.

As shown in Fig. 6, mirror M4 is remotely controllable in pitch and yaw to allow the probe volume image to be scanned over a small area in the vicinity of the aperture. This scheme provides a remote optical alignment capability which can be used to compensate for slight movements of the LDV optical components caused by flexing of the ECS enclosure and sustained periods of low-level vibration.

It should be noted that the effective light-collecting capacity of lens L3 is reduced by the baffle, BT. Without proper baffles, however, photons reflected and scattered by L3 enter the LDV receiver and produce signals comparable in magnitude to the signals resulting from small particles passing through the probe volume. A similar problem is caused by reflected and scattered laser light from tunnel window W2. However, as long as L3 is positioned next to W2, the stray window light is effectively eliminated by the baffle.

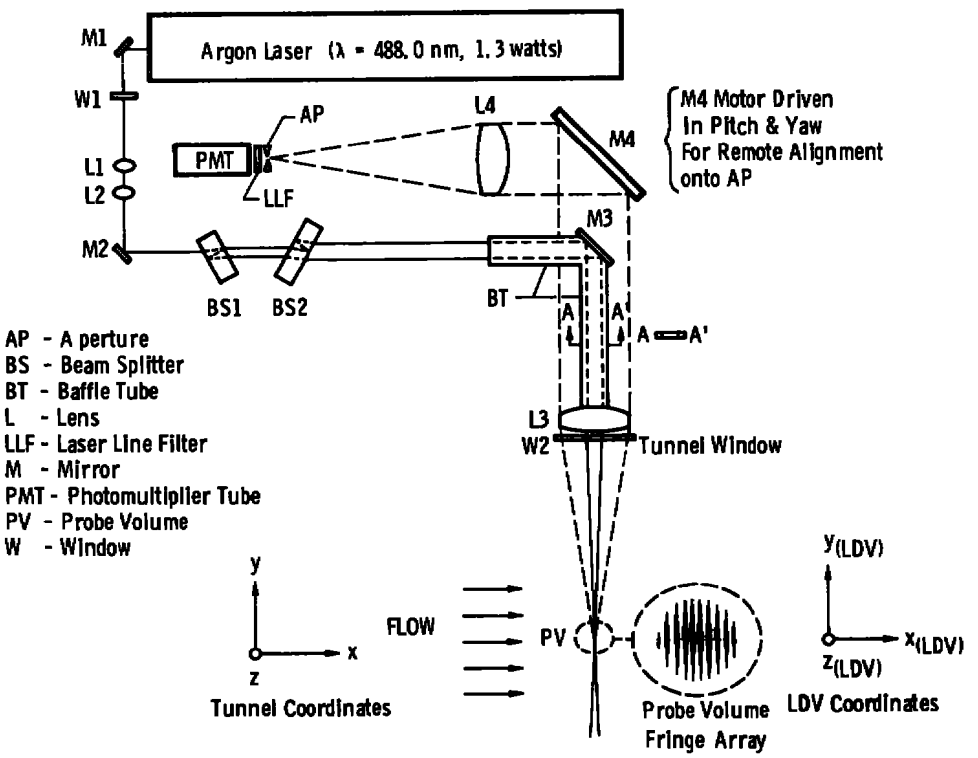

Figure 6. Single-velocity-component LDV optics.

3.3 TWO-VELOCITY-COMPONENT LDV

A unique feature of laser Doppler velocimeters is that they detect only velocities orthogonal to the probe volume fringe planes. Consequently, although a single component system will suffice to measure free-stream velocity if properly aligned with the flow, a second measured velocity component is required if flow angularity in a plane is to be established.

Designing a multicomponent LDV requires that consideration be given to separating the contributions to the detected scattered light arising from each set of fringes. Various investigators have employed separation techniques based on polarization rotation (Ref.

12), optical frequency shifting (Refs. 13 and 14), and color separation (Ref. 15). The last method was chosen for the 4T system because (1) it allows more efficient utilization of available laser power and (2) it permits the use of highly efficient optical filters, thereby minimizing crosstalk between the two velocity signals.

An optical schematic of the two-color, two-component LDV system is shown in Fig. 7. The laser is run in a multiwavelength (nine wavelengths) mode with a total power near 4 watts. Since the powers in the 488.0- and 514.5-nm lines from which the velocity data are obtained are roughly equal, the two-color system has approximately twice the illuminating power of other signal-separating techniques reported in Refs. 12 through 14.

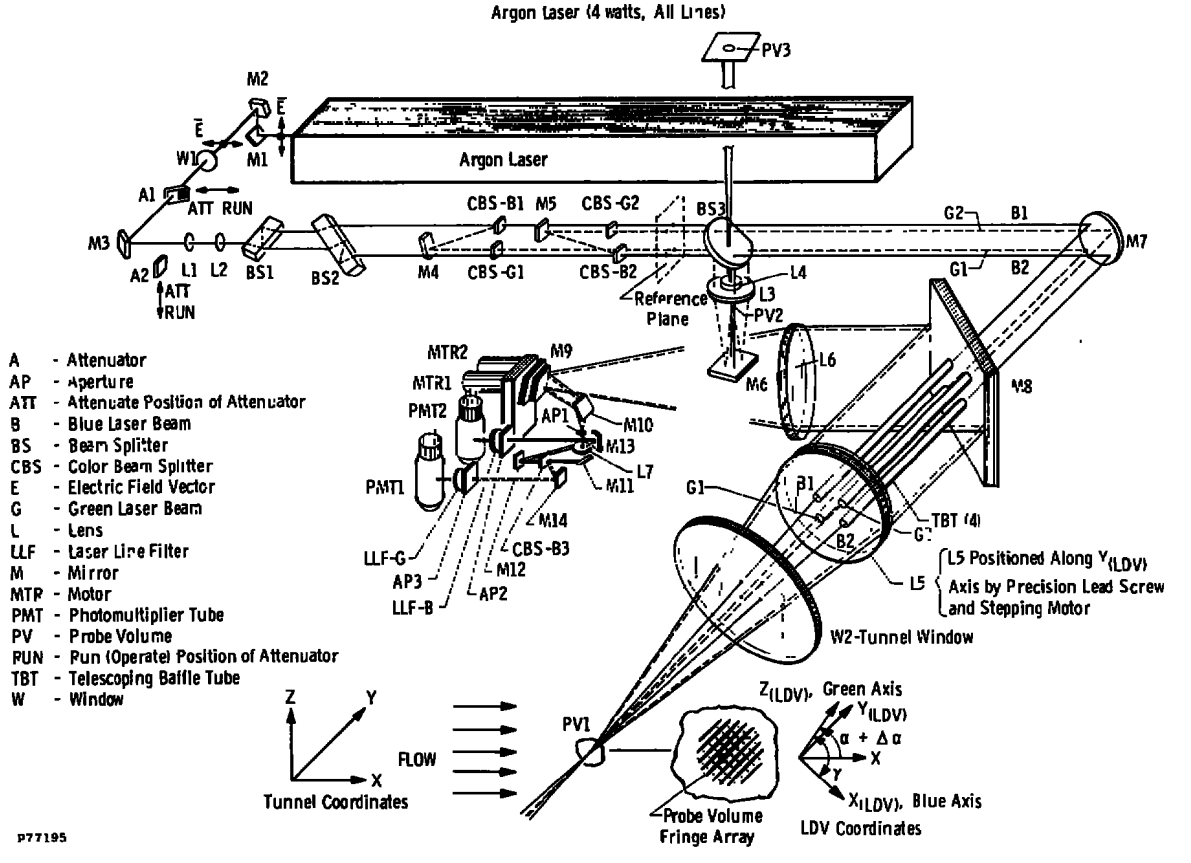

Figure 7. Two-color LDV optics.

As shown in Fig. 7, mirrors M1 and M2 serve to translate the laser beam from the laser compartment through window W1 and into the transmit-receive optics compartment. Attenuators A1 and A2 are used during alignment to reduce the beam intensity to safe eye-viewing levels. Mirror M3 directs the beam to the lens combination L1-L2, which is used for beam expansion. Beam splitters BS1 and BS2 are inclined at 45 deg to the vertical and provide a pair of optical path-length-compensated, two-color beams.

Elements CBS-B1 and CBS-B2 are optical interference filters which transmit the blue, 488.0-nm wavelength light with about 95-percent efficiency and reflect the remaining eight wavelengths with about 99-percent efficiency. Mirrors M4 and M5 redirect the two eight-wavelength beams and cause them to impinge upon elements CBS-G1 and CBS-G2. These elements are optical interference filters which transmit the green 514.5-nm wavelength and reflect the remaining seven wavelengths. All the color separation elements are mounted on a temperature-controlled platen maintained at 110°F, the highest temperature usually encountered in the 4T plenum region.

The beam splitter BS3 diverts 1 percent of the radiation onto an optical assembly consisting of elements BS3, M6, L3, and L4 in order to create the probe volumes PV2 and PV3. Probe volume PV3 is a magnified equivalent of the measurement volume and is projected onto the upper plenum wall in 4T for alignment purposes. The parallelism of the four transmitted beams is adjusted while fringe quality is viewed in PV3. In this manner a critical optical alignment can be effected without the necessity of projecting beams into the tunnel test section, which is often occupied by tunnel personnel.

Mirror M7 effects a 90-deg beam direction change and directs the four-beam array through the telescoping baffle tubes, TBT, which pass through holes drilled in mirror M8 and are cemented into annuli bored into lens L5, the common transmitter-receiver lens. The baffle tubes prevent light that has been scattered and reflected by lens L5 from entering the receiver.

Lens L5, which has a 5-in. diameter and a 25-in. focal length, is mounted on a platform positioned by a precision lead screw and stepping motor. Movement of L5 causes the probe volume to traverse along the y-axis direction. The total possible travel is 16 in. The traverse mechanism can be programmed to step in integer multiples of 0.00025 in. The position error is no greater than ±0.0005 in. for each 12 in. of travel. Additional details of the traverse system are shown in Figs. 8a and b.

The transmitted four-beam array (B1, B2, G1, and G2) emerging from the baffle tubes passes through window W2, which is flush mounted with the test section porous wall (Fig. 8c), and intersects to form the measurement probe volume PV1. Two sets of nominally orthogonal fringes are formed within the probe volume. The green fringes have a spacing of 8.8 μm and are inclined at a nominal 45 deg to the tunnel x-axis coordinate (Fig. 7) while the blue fringes are spaced at 8.5 μm and inclined at a nominal -45 deg to the x-axis. The fringe planes were inclined in order to equalize the number of velocity samples obtained by each component of the LDV to 1) increase the probability that each velocity component was measured simultaneously, 2) maximize the data rate of the system, and 3) eliminate the flow direction "dead zone" (Ref. 12). It can be shown (Ref. 16) that a system configured like the present two-color LDV gives the instantaneous

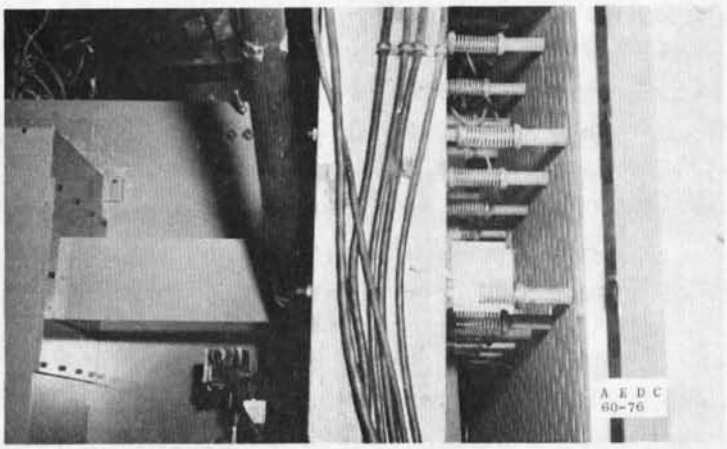

a. View of lens traverse unit from top of 4T test section

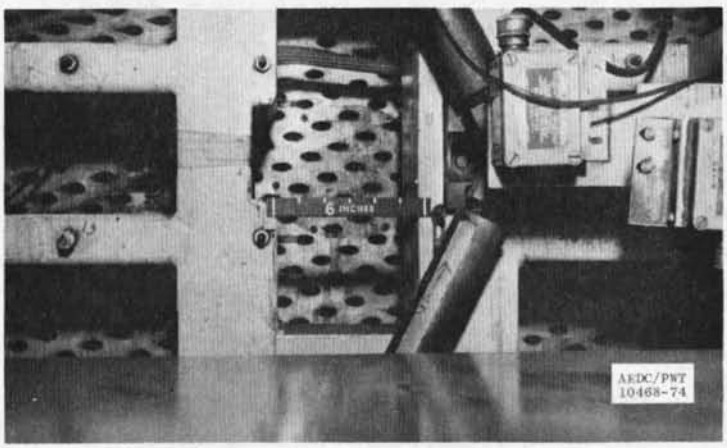

b. Access port for lens traverse unit

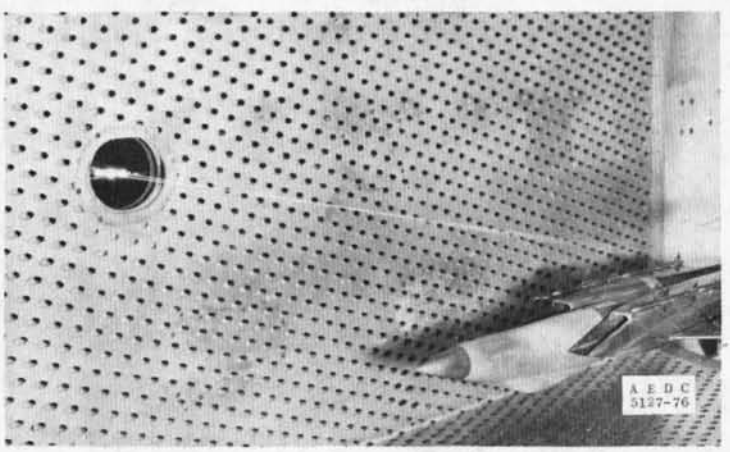

c. Optical entry into the 4T test section

Figure 8. Details of the LDV/ECS assembly.

velocities, mean velocities, and turbulent intensities along the (x and z) axes, as well as flow angularity and Reynolds stresses for the x-z plane. Window W2 was specially prepared for this application since surface nonuniformities, scratches, and adhering particles can shift the spatial orientation of the probe volume fringes by several tenths of a degree. The window characteristics are summarized in Table 1.

Table 1. LDV Window Characteristics

Material	Schott BK-1
Diameter	6 in.
Thickness	3/8 in.
Surface Flatness	0.1μm/surface
Surface Parallelism	±0.010 in.
Surface Scratch-Dig Factor	60-40
Coating (λ = 0.5μm)	Dielectric V Coat
Reflectance (λ = 0.5μm)	0.0025/surface

The 488.0- and 514.5-nm-wavelength laser light backscattered from particles traversing the probe volume, PV1, passes through window W2 and is collimated by lens L5 as shown in Fig. 7. The collimated light is turned through 90 deg by reflection from mirror M8 and is brought to a focus by lens L6 after being reflected from mirrors M9 and M10. Proper optical alignment requires that the focus of L6 be coincident with the 200-μm opening in aperture AP1. This alignment can be achieved remotely by moving mirror M9 in pitch and yaw by motors MTR1 and MTR2 until maximum amplitude signals are observed from PMT1 and PMT2.

Aperture AP1 is used as a spatial filter to eliminate some of the objectionable light reflected and scattered by window W2 as well as stray light from test section illumination lamps. After passing through AP1 the received light is collimated by lens L7 and turned through 90 deg by mirror M11. The blue and green light is then separated by color beam splitter CBS-B3. The blue light is directed to AP2 by mirrors M12 and M13. The blue light then passes through AP2 and LLF-B and impinges upon the photocathode of PMT2. The green light is similarly directed to PMT1.

It should be noted that one deficiency of the present system is the inability of the baffle tubes to intercept stray light when lens L5 is traversed back from the window. This problem becomes severe when the lens is more than 5 in. away from the window, whereupon the amplitude of the reflected light becomes comparable to the amplitude of the signals obtained from the probe volume. To compensate for this difficulty, attention will be given in future studies to designing a window containing a hole pattern capable of passing the four transmitted beams.

A photograph of the two-color optics installed in the 4T ECS enclosure is shown in Fig. 5. An electrical connector panel, shown in the upper right portion of Fig. 5, is used to connect instrumentation leads from the transmit-receive optics compartment to the laser compartment. Instrumentation cables are connected to this panel and passed through the flexible conduit to the operator's station.

A minimum number of optical components were used in the design of the LDV system in order to minimize the optical power losses caused by reflection at each air-glass interface. High efficiency, dielectric coatings were applied to all optical surfaces to further reduce losses.

3.4 LDV SIGNAL PROCESSORS

In an LDV application using natural particulates, photodetector signals will be observed that vary in level from single photon-detected events up to thousands of photo-detected events per fringe crossing. Since it can be stated with some generality that, for a given optical system, the total light scattered by the particles is directly proportional to particle size, it is clear that many photon-limited events observed at the PMT are caused by scattering by small particles traversing the probe volume. It is desirable to be able to derive velocity information from these low-level signals because 1) intrinsic small particles are more numerous than larger ones, and 2) in flow regions with appreciable velocity gradients, the small particles will respond more rapidly and thus will more nearly approach the local fluid velocity. Accordingly, a new type of data processor, the Doppler Data Analyzer (DDA), was developed in the course of the 4T program and has the capability of processing much lower level signals than the Model 8 Doppler Data Processor (DDP) that has been conventionally used at AEDC. Both types of processors were used in the experimental program and are described below.

3.4.1 Model 8 DDP

The Model 8 DDP (Ref. 17) is a burst counter which determines the average period of a Doppler burst by measuring the duration of eight consecutive signal cycles with a 125-Mhz clock. The instrument is capable of processing signals from 15 kHz to 100 MHz, utilizing eight overlapping frequency ranges. For the 10- to 50-MHz range used in this investigation, pulse stretching is used to give a time resolution of 0.01 nsec, but this limits the maximum data rate to 45 kHz. The DDP has error control logic that allows it to reject distorted signals caused by a high noise content or pulse dropout by requiring the four- and five-cycle counts to be 4/8 and 5/8 of the eight-cycle count to within a maximum tolerance of 3 percent.

The characteristics of the Model 8 make it of limited utility in processing low-level signals. First, since an oscilloscope sweep pulse is required to activate the DDP, a signal is not processed unless it exceeds the oscilloscope trigger level. This eliminates extremely small particles or even moderately sized particles if the threshold is set too high. Second, the Gaussian intensity profile across the probe volume causes the signal amplitude to vary as a particle crosses the probe volume. For small particles the signal may exceed the threshold level only when the particle is in the central region of the probe volume, with the result that the required eight cycles of signal may not be produced. Finally, photon-limited signals are readily obscured by spurious photon-detected events, thus increasing the probability that the error control logic will reject the samples as being invalid.

3.4.2 Doppler Data Analyzer

The DDA shown schematically in Fig. 9 consists basically of signal-conditioning electronics and two independent data processing channels which compare signal duration to counts of a 500-MHz clock. Each channel interacts with individual high speed, 8-bit, bipolar microcomputers (Microcomputer Nos. 1 and 2) which array individual burst durations in a histogram format. The histogram format is programmable, and for the 4T studies displayed the number of observations obtained in each of 64 cells having a bin width of 2 nsec. A histogram was completed in the 4T studies when the number of samples obtained in any cell reached 256. This number can be varied over the range from 16 to 256 samples in steps of 2^n. When the appropriate condition is satisfied, the histogram is displayed on a CRT and the contents of the histogram random access memory (H-RAM) are transferred to a first-in, first-out memory (OUT-FIFO). Data from the OUT-FIFO are subsequently transferred to a 16-bit microcomputer (Microcomputer No. 3) which stores the histogram data and performs the calculations described below.

The DDA is programmed to store the total duration, PT_{ij}, of a burst containing, as desired, P = 1, 2, or 4 cycles of information with period T_{ij}. An average burst duration for the j^{th} histogram is accordingly computed and stored by Microcomputer No. 3 from the relation

$$\overline{PT}_j = \frac{1}{N} \sum_{i=1}^{N} PT_{ij} \qquad (1)$$

where N is the total number of samples contained in the five histogram cells centered about the cell containing the required 2^n samples. Therefore, N may vary from 16 to 1,276 samples according to the standard deviation of the data and the criterion selected for histogram termination. This feature of the DDA may be regarded as a form of error

control since it is expected that burst data obtained over a short time interval should exhibit a strong central tendency and, it may be argued, signals whose periods are greatly different from the mode of the histogram generally arise from random errors or pulse dropout or addition.

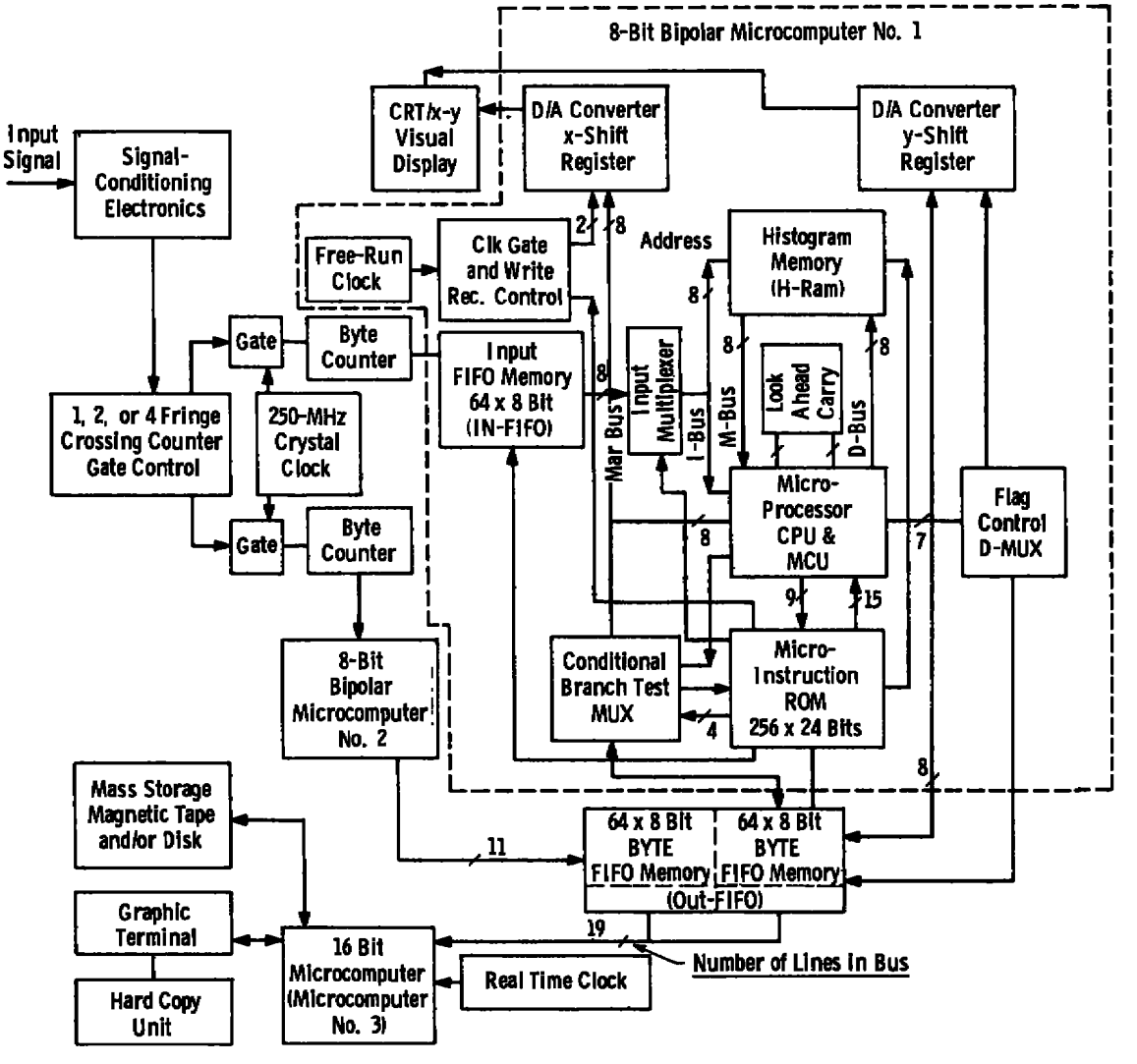

Figure 9. Doppler Data Analyzer.

An average duration for the M histograms stored by Microcomputer No. 3 is also computed and is given by the relation

$$P\bar{T} = \frac{1}{M} \sum_{j=1}^{M} P\bar{T}_j \qquad (2)$$

where M may be programmed for any number of histograms in the range $1 \leqslant M \leqslant 1{,}000$. A final computation gives the mean period for the entire data set by dividing Eq. (2) by the appropriate value for P.

It should be noted that the DDA has several features which give it an extremely high data acquisition capability. When the two independent signal-processing channels are multiplexed through a counter gate control, one channel acquires a sample, PT_{ij}, while the second processes the previous sample, $PT_{i-1,j}$. A sample for the DDA, however, may consist of only a portion of the Doppler burst so that several samples may be obtained from a single particle. Internally, it requires only 12.6 μsec to transfer data from H-RAM to OUT-FIFO memory and to activate the CRT. Each IN-FIFO can further transfer 8-bit bytes at a 15-MHz rate while Microcomputer Nos. 1 and 2 transfer data to the correct H-RAM memory at a 3.33-MHz rate. For a continuous-wave 50-MHz input signal, these features permit the DDA to produce histograms at a rate of 40 KHz so that a limited duration velocity sample rate in excess of 10 MHz is possible. In wind tunnel applications, velocity sample rates approaching 300 kHz have been observed (Ref. 18) using only intrinsic particulate matter. It is clear, therefore, that in highly seeded flows quasi-instantaneous velocity measurements can be obtained, giving the DDA a potential for performing moderately high frequency turbulent flow diagnostics.

The Model 8 DDP is restricted in its ability to process low-level signals due to dependence on an oscilloscope sweep trigger level, the necessity of counting eight cycles of the burst signal, and the error control logic employed. The DDA is free of these restrictions, and its capabilities for low-level signal processing are further enhanced by the signal-conditioning electronics indicated in Fig. 9. In this module signals are passed through an attenuator-amplifier device and then through a highpass-lowpass filter combination. For the 4T program, 10-MHz highpass and 50-MHz lowpass filters were employed. After the signal was filtered, a logarithmic compression amplifier was used to equalize the signal amplitudes of photon-limited or fully resolved events. Two additional stages of amplification were then used prior to entering the zero-crossing detector. Although filtering of the input signal tends to inhibit noise at frequencies differing vastly from the expected range of Doppler burst frequencies, the signal and noise components of in-band waveforms experience equal amplification. Time interval averaging of many samples by the DDA [Eq. (1)] enhances the resolution of the period measurement, thereby reducing the measurement uncertainty caused by noise-induced precision errors (Ref. 16)and time resolution factors (Ref. 19). This was substantiated experimentally by bench tests utilizing controlled levels of additive noise. Such tests clearly showed that the uncertainty associated with the averaged data was significantly less than that associated with individual period measurements.

3.5 INSTRUMENTATION AND CONTROLS

A block diagram of the data acquisition system, electronic instrumentation, and controls is shown in Fig. 10. The computer, discussed further in Section 3.6, has a 32K memory supplemented by a 4.9-megabyte disk memory unit. For data sets consisting of data from both DDP's and the digital clock, a data throughput rate of 36,000 sets per second can be achieved. The time resolution of the digital clock is 1 msec. An interactive program with several options is used to permit adaptation of the LDV system to

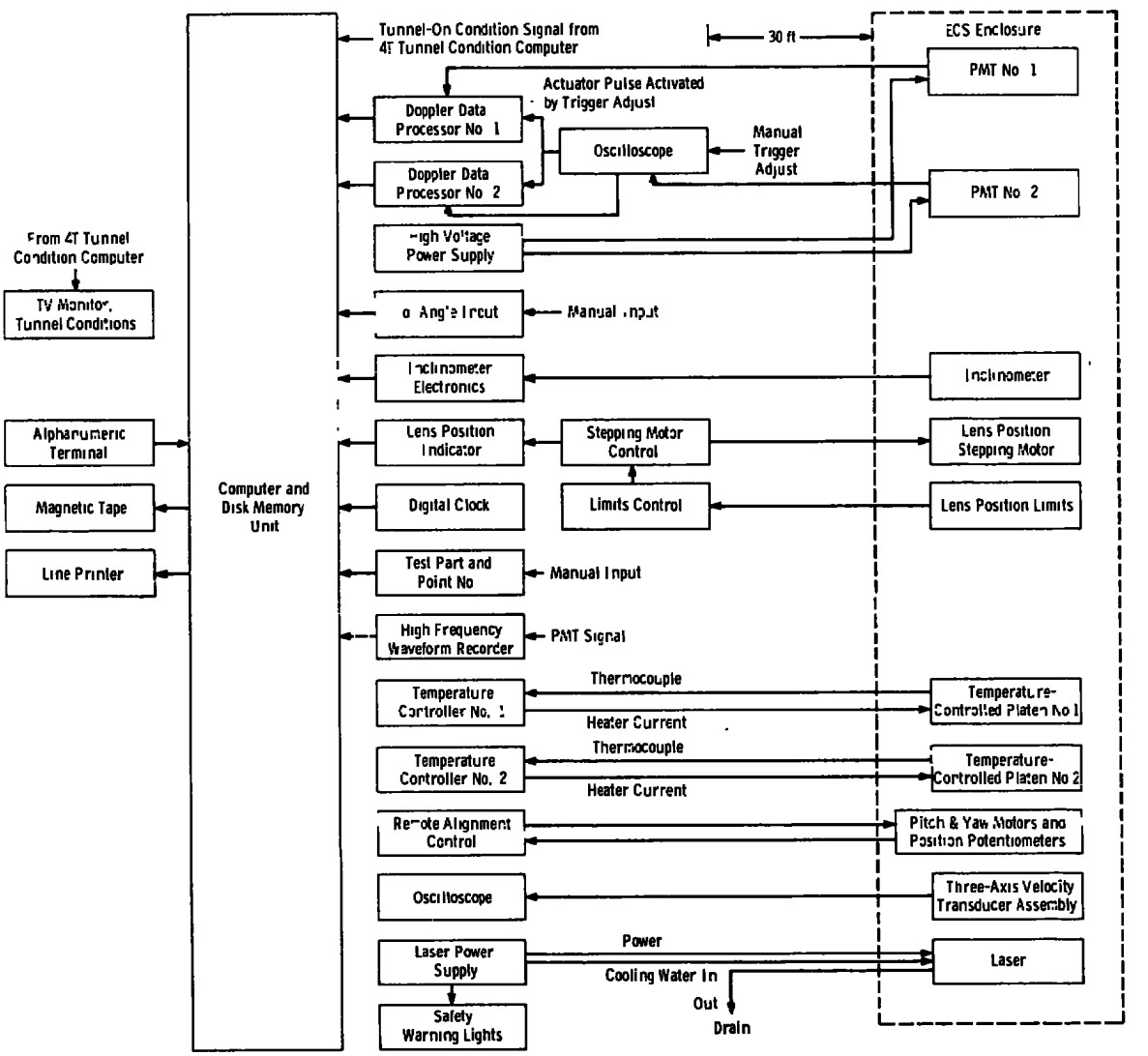

Figure 10. Block diagram of computer-based data acquisition system, electronic instrumentation, and controls.

particular test requirements. Program options are entered by the alphanumeric terminal, and data are permanently recorded on magnetic tape for later reduction. On-line data are provided by the line printer.

The 4T test section free-stream Mach number is computer controlled to within ±0.005. When the Mach number is outside this tolerance, an inhibit signal is sent to the LDV data acquisition system. This inhibit signal suspends acquisition of LDV data until the tunnel is brought back to the proper operating conditions.

The α angle input device is used to manually enter the static inclination angle of the velocity component measurement axis defined by the green fringes (see Fig. 7). Small angular changes, $\pm\Delta\alpha$, about α are measured by the inclinometer and its associated electronics. The inclinometer is oriented to measure the pitching motion of the ECS/LDV system. The inclinometer-electronics combination has a full-scale measurement capability of ±1 deg with a resolution of 0.001 deg.

The stepping motor is used in conjunction with a precision lead screw to position the transmit-receive lens (lens L5, in Figure 7). The stepping motor control unit can be programmed to traverse lens L5 in integer multiples as small as 0.00025 in. Lens position is determined by an up-down counter device identified as the lens position indicator. Lens L5 is automatically stopped at the extremes of its travel by the lens position limits and the limit control.

The high-frequency waveform recorder is a 500-MHz bandwidth device and is used primarily for PMT signal waveform recording. Either of two different computer programs may be selected to operate either the waveform recorder or the data acquisition system.

The temperature controllers are used to regulate the electric current through heaters mounted on the temperature-controlled platens. Thermocouple sensors furnish input signals to the controllers, which hold the platen temperature to within about ±2°F of a 110°F set point. The color beam splitters, mounted on the platens, require a temperature stability of about ±5°F about the set point to maintain proper optical alignment.

The remote alignment control is used to supply power to the alignment motors, MTR1 and MTR2, shown in Fig. 7. These motors drive jackscrews which in turn move mirror M9 (Fig. 7) to implement the remote optical alignment scheme. The position of M9 is sensed by two potentiometers whose output is displayed by two analog voltmeters.

The functions of the remaining instrumentation and control components may be readily determined by a study of Fig. 10.

3.6 DATA ACQUISITION SYSTEMS

Two computer-controlled data acquisition systems were designed and built for the LDV development and applications programs at AEDC. Both systems use a 16-bit minicomputer as the system controller. The basic system block diagram is shown in Fig. 11. Source and object programs prepared on another system are loaded by the paper tape reader. The magnetic tape is used to record large amounts of data for processing by a large-scale computer. Data needed during LDV system operation are displayed by the line printer. The alphanumeric terminal serves as the man-machine interface for entering commands and interrogating the computer program. This terminal is also useful for perfecting new programs. The maximum possible core memory of 32K words is included with both systems to achieve as much buffer space for data as possible. A magnetic disk was added to the 4T system for use as a high capacity data buffer and to provide for more convenient programming of both computer systems.

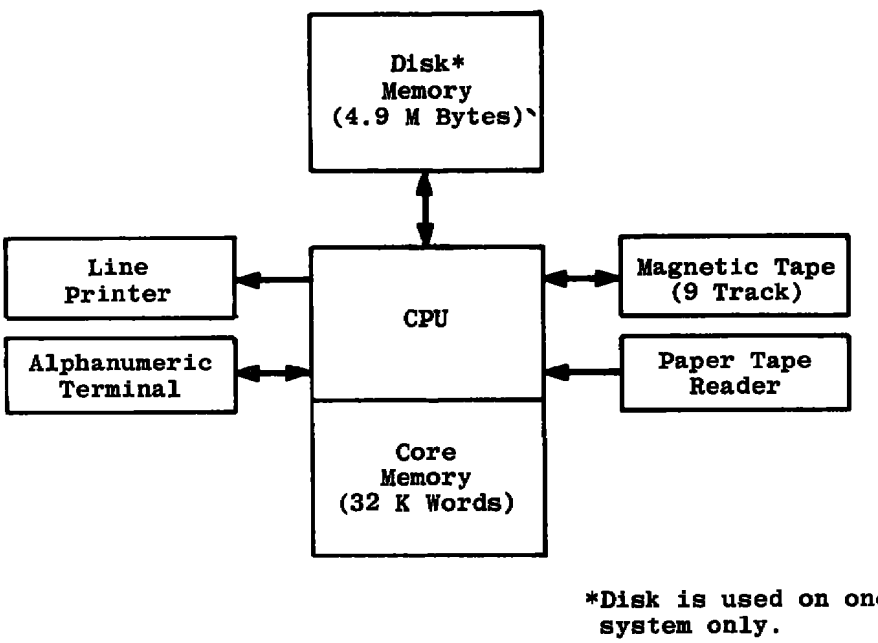

Figure 11. Block diagram of minicomputer system.

A 16-input, 16-bit digital multiplexer was designed and fabricated to facilitate the input of all LDV system data sources through one input/output channel. Some of the data inputs require more than 16 bits and therefore use two of the 16 available input channels.

LDV signals encountered in applications at AEDC range in frequency from 10^3 to 10^8 Hz. The capability to record LDV signal waveforms for subsequent study contributes

to signal processor development efforts. A high-frequency waveform recorder was interfaced to the 4T computer system. The waveform recorder utilizes a scan-converter device consisting of a 10-kv electron gun which writes a charge image of the signal waveform onto a target composed of an array of silicon diodes. The diodes are spaced on nominal 0.0005-in. centers, and the entire diode array measures 3/8 in. by 1/2 in. The x and y coordinates of the charged diodes are stored in a 4K work (10-bit) memory. This information is made available for transfer to the computer on command. The maximum sweep rate obtainable is 0.5 nsec per division, with the result that 500-MHz signals can easily be recorded.

The time required for acquisition of the x-y coordinate information by the computer is determined by the load and read cycle times. The load cycle is the time required to digitize the x-y coordinate data and store this data in the 4K memory and is typically 60 to 70 msec. The read cycle is a function of the computer and program. The maximum read rate is 1.6 μsec per word. A waveform is typically described by about 1,600 words, and the corresponding maximum read cycle time is about 2.5 msec.

An electronically generated graticule can be superimposed on the recorded waveform. However, this adds to the read cycle time because it increases the number of words required to describe the trace. Voltage and time scale factor information is converted to 32 ASCII words and is available for presentation at the end of a read cycle. This operation also adds to the total time required per waveform recording.

The waveform recorder, when under computer control, responds to the following sequential commands: (1) select digital mode (computer control); (2) arm single sweep; (3) select graticule generator; (4) lock memory; (5) inhibit ASCII data; (6) load recorder memory; (7) read recorder status; (8) read data; and (9) clear recorder.

4.0 PROCEDURES

One of the objectives of this study was to determine the uncertainties associated with the LDV measurements. This required the development of exacting calibration and data reduction procedures. The largest uncertainties in the measurements are shown to be attributable to the calibration techniques, with lesser uncertainties caused by the time interval resolution characteristics of the counter-type signal processor.

4.1 CALIBRATION

The 4T LDV is a dual scatter system (Refs. 20 and 21) in which two laser beams intersect to form a region of interference fringe planes as shown in Fig. 7. The Doppler shift frequency obtained by a dual scatter LDV is given by

$$f_D = \frac{1}{2\pi} \vec{V} \cdot (\vec{k}_2 - \vec{k}_1) \tag{3}$$

where $\vec{V}$ is the velocity vector of the light-scattering particle, $\vec{k}_1$ is the wave vector of one of the incident beams, and $\vec{k}_2$ is the wave vector of the second beam. This equation can be put into the form

$$\vec{V} \cdot \vec{u}_\perp = \frac{\lambda}{2 \sin \frac{\theta}{2}} f_D \tag{4}$$

or

$$\vec{V} \cdot \vec{u}_\perp = K_V f_D \tag{5}$$

where λ is the wavelength of the incident laser light, θ is the angle subtended by the intersecting beams, $\vec{u}_\perp$ is a unit vector normal to the fringe planes, and K_v is the LDV calibration factor or, equivalently, the fringe spacing. Equations (4) and (5) show that only the velocity component normal to the fringe planes is measured and that it varies linearly with the Doppler shift measured by the signal processor. Accurate determination of velocity, however, requires measuring either the angle between the intersecting beams or the fringe spacing to a high degree of accuracy. For the two-color system, moreover, the orientation of the fringes with respect to a reference axis, and the angle between the two sets of fringes must also be determined.

Figure 12 depicts one procedure used with the two-color LDV to determine the intersection angles θ_B and θ_G. A mirror was used to deflect the four-beam pattern by 90

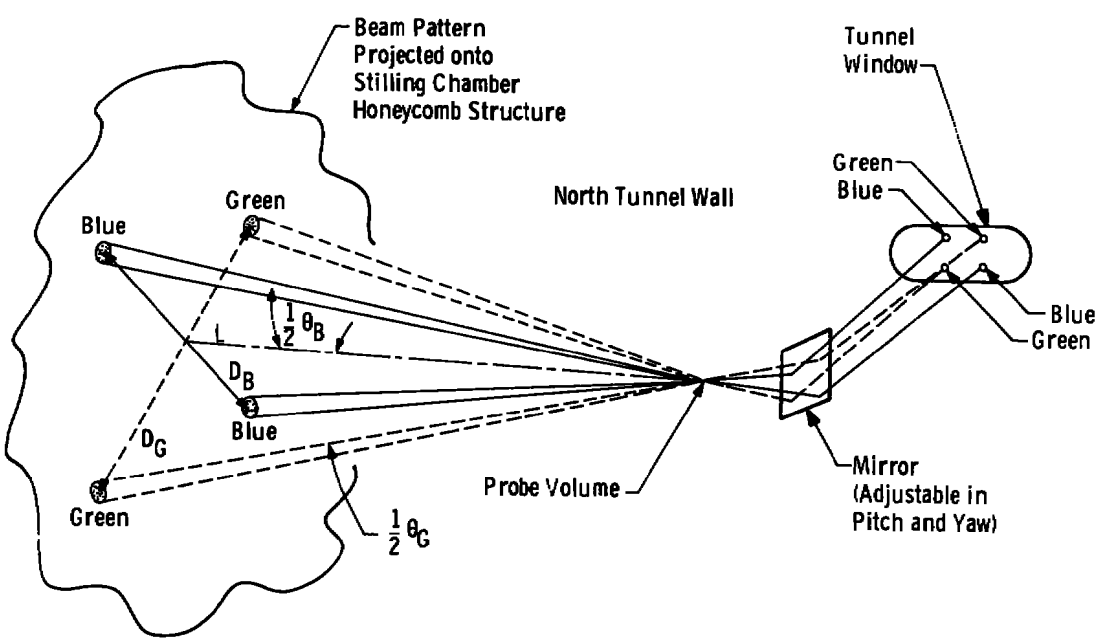

Figure 12. Geometric determination of LDV calibration factor.

deg, and the mirror pitch and yaw position adjustments were manipulated to orient the optical axis parallel to the test section walls. The beam separation was thereby increased as the beams propagated through space and terminated on the honeycomb structure located in the tunnel stilling chamber. From Fig. 12 and Eq. (5) it is seen that the LDV calibration factor can be found by substituting the measured lengths L, D_B, and D_G into the following relationship:

$$K_v = \frac{\lambda}{2 \sin \left[\tan^{-1} (D/2L)\right]} \tag{6}$$

The uncertainty in determining K_v is caused primarily by random errors introduced in measuring D because the four beam spots shown in Fig. 12 are irregularly shaped due to diffraction effects. Therefore, a subjective decision is involved in choosing the spot centers.

It can be seen from Fig. 12 that the spatial orientation of the green and blue fringe planes can also be obtained from simple geometric considerations using this approach. An alternate procedure for determining the fringe pattern orientation was used, however, and is illustrated in Fig. 13. A mirror was used to deflect the transmitted 4-beam pattern by

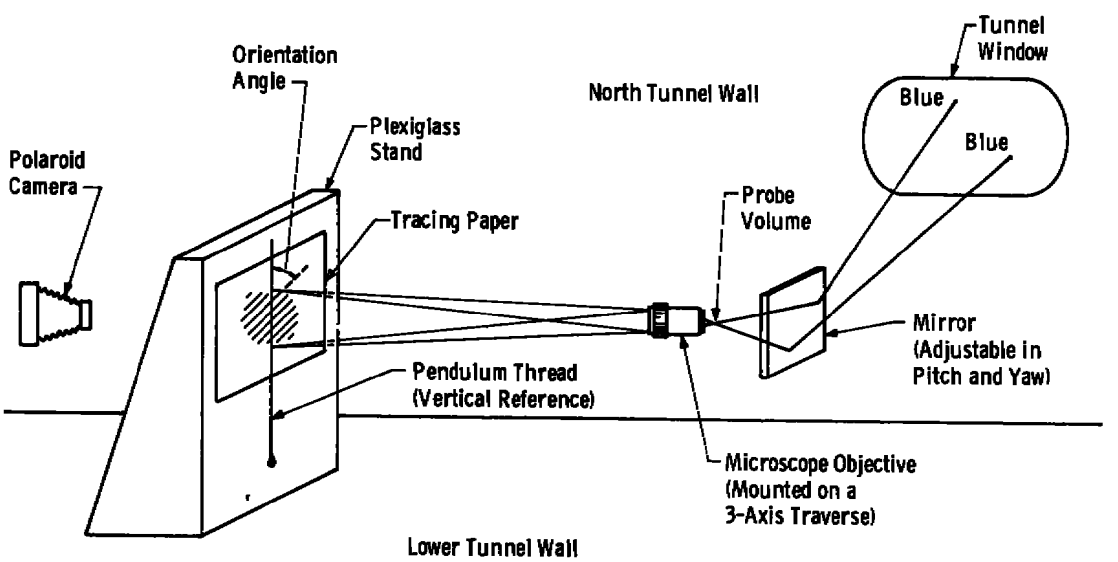

Figure 13. Apparatus for photographing the LDV fringe pattern with vertical reference line.

90 deg so that the probe volume image could be projected onto tracing paper by a microscope objective. With the green beams blocked, a polaroid camera was used to photograph the blue fringes along with the superimposed vertical reference line furnished

by the pendulum support thread. The green fringes were then photographed with the blue beams blocked. A typical photograph is shown in Fig. 14 along with a transparent overlay containing scribed parallel lines. By aligning the scribed lines with the fringes, the orientation angle, α, of the green fringes with respect to the vertical reference line was determined from $\alpha = \tan^{-1}(y/z)$. A similar procedure was used to determine the orientation angle, β, for the blue fringes. The intersection angle, γ, for the set of nominally orthogonal fringes is, therefore, $\gamma = \alpha + \beta$.

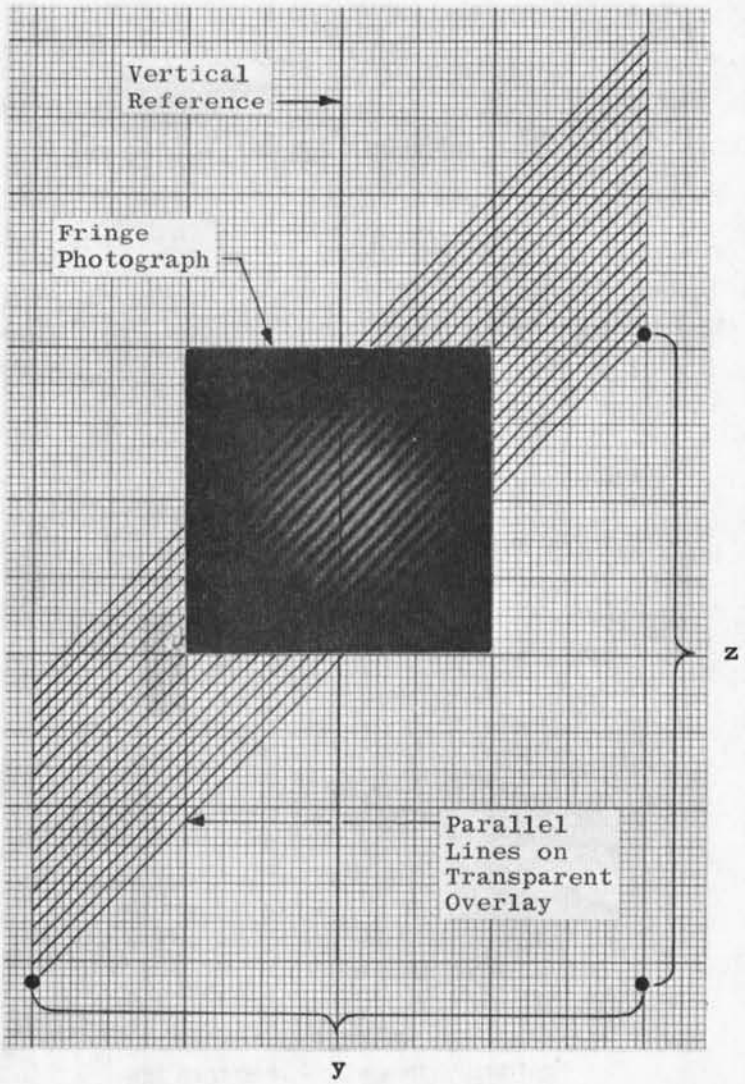

Figure 14. Photographic determination of fringe orientation angle.

4.2 DATA REDUCTION

The 4T reference coordinate system is the orthogonal Cartesian System (x, y, z) shown in Figs. 3, 6, and 7. The instantaneous velocity components along these component axes are u, v, and w, respectively. The single-velocity component LDV system was used to measure the u, or axial, component of velocity from which the mean and root-mean-square (rms) velocities were calculated. The two-velocity-component LDV was used only to measure the resultant mean velocity magnitude and flow angle in the x-z plane, although, as noted earlier, other information could be derived from the data obtained. The following descriptions of data reduction procedures apply only to the Model 8DDP data since the prototype DDA signal processor was used as a stand-alone instrument using the data reduction routines described in Section 3.4.

4.2.1 Single-Velocity-Component LDV

The Reynolds model for turbulent fluid flow suggests decomposing the instantaneous velocity as

$$u = \bar{u} - u' \tag{7}$$

where $\bar{u}$ is the mean velocity and u' is the instantaneous deviation from the mean. For N instantaneous, true velocity samples, u_i, the mean velocity, $\bar{u}$, is given by

$$\bar{u} = \lim_{N \to \infty} \frac{1}{N} \sum_{i=1}^{N} u_i \tag{8}$$

The rms fluctuation velocity, u*, is defined by

$$u^* = \left[\lim_{N \to \infty} \frac{1}{N-1} \sum_{i=1}^{N} (u_i - \bar{u})^2 \right]^{1/2} \tag{9}$$

The relative turbulence intensity, σ, in a flow with average velocity $\bar{u}$ is given by (Ref. 22)

$$\sigma = \frac{1}{\bar{u}} \left(\frac{\overline{u'^2} + \overline{v'^2} + \overline{w'^2}}{3} \right)^{1/2} \tag{10}$$

For locally isotropic turbulence such as is to be expected in the free stream of Tunnel 4T, Eq. (10) reduces to

$$\sigma = \frac{u^*}{\bar{u}} \tag{11}$$

Because of the finite sample size and various bias and precision errors, the velocities measured by any instrument can provide only estimates of the true statistical characteristics of a flow. An estimate, $\bar{V}_x$, of the true mean axial velocity can be computed from a finite set of N LDV velocity samples by

$$\bar{V}_x = \frac{1}{N} \sum_{i=1}^{N} V_{x_i} \tag{12}$$

At present in 4T, the LDV cannot distinguish velocity fluctuations caused by turbulent flow from unsteady tunnel operations. During normal tunnel operation, Mach number is held to within ±0.005 of a particular set point, which results in a possible maximum velocity fluctuation of ±1 percent at Mach Number 0.5 and about ±0.4 percent at Mach Number 1.2. Therefore, the velocity variation parameter measured by the 4T LDV will be termed the estimated relative turbulence intensity defined by

$$\hat{\sigma} = \frac{V_x^*}{\bar{V}_x} \tag{13}$$

where the fluctuation velocity is given by

$$V_x^* = \left[\frac{1}{N-1} \sum_{i=1}^{N} \left(V_{x_i} - \bar{V}_x \right)^2 \right]^{1/2} \tag{14}$$

4.2.2 Two-Velocity-Component LDV

It is obviously desirable for a multicomponent LDV to have orthogonal measurements axes. However, the measurement axes of virtually all two- and three-component LDV systems deviate from the desired orthogonal condition to some extent. This nonorthogonality can be ignored for many applications because the resultant measurement errors can be tolerated. However, for the 4T LDV System, velocity magnitude errors in the range of 1 percent and flow angle errors in the range of several tenths of a degree resulted when axis nonorthogonality was not accounted for. Such error magnitudes are not acceptable, and measurement axis nonorthogonality must be considered in the two-component data reduction routine.

In Fig. 15, the directed line segment, $\vec{V}$, represents the x-z plane velocity vector of a discrete particle passing through the LDV probe volume at angle ϕ. The transmitted 4-beam array forms measurement axes which are represented by the lines connecting the pairs of Blue and Green spots. The particle velocity component along the Blue axis is designated V_B, and that along the Green axis is V_G. The angle γ is equal to the sum of

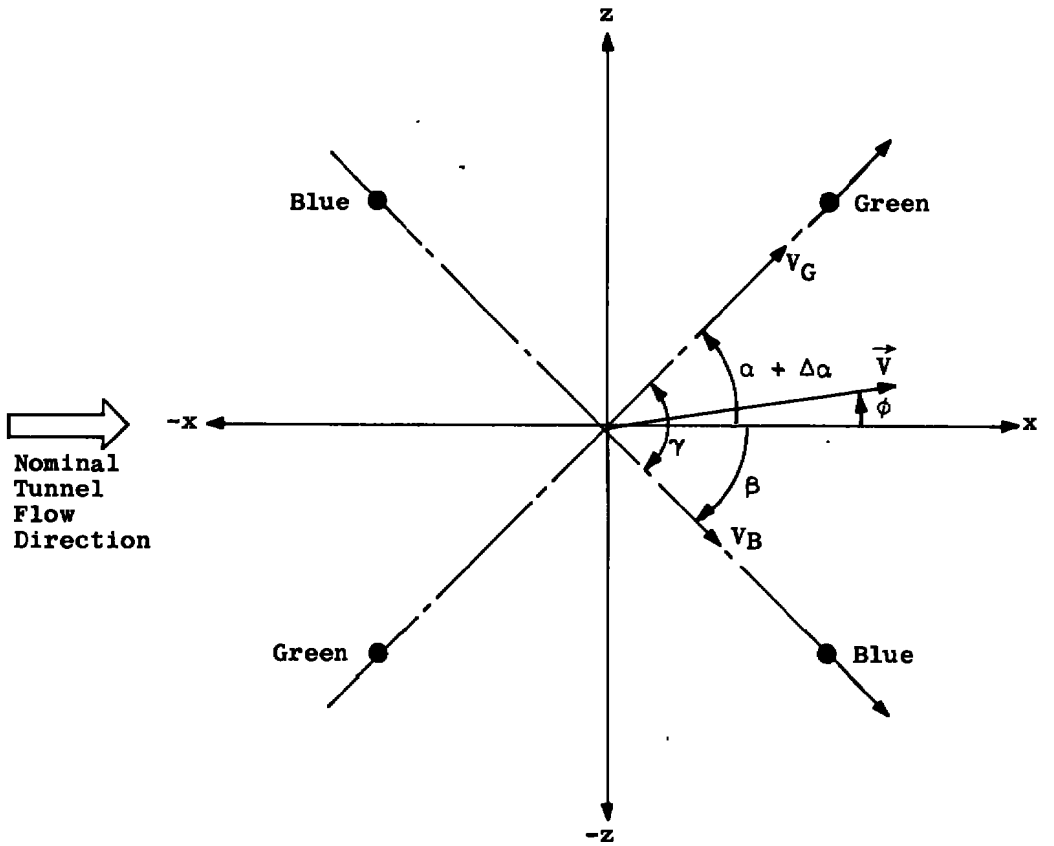

Figure 15. Geometric relationship of velocity vector $\vec{V}$ and LDV measurement axes.

the angles α and β determined by calibration. An angle $\Delta\alpha_i$ is associated with each measurement because of small vibration-induced motions of the ECS/LDV system. A study of the geometric details of Fig. 15 and straightforward application of trigonometric relationships yields the velocity magnitude and flow angle in terms of measurable LDV system parameters. The expression for velocity magnitude is

$$V_{xz} = \left[\left(\frac{V_G - V_B \cos\gamma}{\sin\gamma}\right)^2 + V_B^2\right]^{1/2} \tag{15}$$

whereas the expression for flow angle is

$$\phi = (\alpha + \Delta\alpha) - \cos^{-1}\left(\frac{V_G^2 \sin^2\gamma}{V_G^2 - 2V_B V_G \cos\gamma + V_B^2}\right)^{1/2} \tag{16}$$

When $\gamma = 90$ deg, these two equations simplify to

$$V_{xy} = \left(V_G^2 - V_B^2\right)^{1/2} \tag{17}$$

and

$$\phi = (\alpha + \Delta\alpha) - \cos^{-1}\left(\frac{V_G}{V}\right) \tag{18}$$

For mean velocity magnitude and flow angle determinations, V_B, V_G, and $\alpha + \Delta\alpha$ are replaced in Eqs. (15) through (18) by their arithmetic mean values:

$$\bar{V} = \frac{1}{N}\sum_{i=1}^{N} V_i \tag{19}$$

$$\alpha + \overline{\Delta\alpha} = \alpha + \frac{1}{N}\sum_{i=1}^{N} \Delta\alpha_i \tag{20}$$

4.3 MEASUREMENT UNCERTAINTIES

The uncertainty in the value obtained for the velocity or flow angle measured by an LDV is dependent upon many factors. Two of the most difficult to assess are errors resulting from particle-fluid interaction dynamics and the possible statistical bias of the data due to the inherent sampling characteristics of laser velocimeters. In the latter case, it has been shown that arithmetic averages of individual LDV velocity samples provide the best estimates of the true, time-averaged velocity provided that the velocity sampling process is random in time (Ref. 23). If, however, the time interval between velocity samples is proportional to the instantaneous fluid velocity, a statistical bias (Ref. 24) will result, with the effect that arithmetic averages will overpredict the mean and underpredict the rms value (Refs. 16 and 23). Reference 16 suggests that statistical bias will occur only when the LDV data acquisition rate is high. The data acquisition rate in 4T was low compared to turbulent fluctuation rates, and no clear evidence of statistical bias effects was observed.

An experiment described in Section 5.2 was performed to investigate particle-fluid interaction dynamics. This experiment indicated that the intrinsic particulate matter in 4T is small enough that particle inertial lag effects could be neglected for the free-stream mean velocity measurements. Because of these observations it was deemed unnecessary to compensate the 4T LDV data for statistical bias and particle lag effects.

As with measurements of any physical quantity, instrument bias and precision errors are associated with quantities derived from LDV data. Instrument bias refers to those systematic errors that are not eliminated by calibration procedures, whereas precision errors are random in nature and are related to the repeatability of the measuring system. Procedures for quantitatively evaluating the resulting uncertainty in a measured quantity due to bias and precision errors are given in Refs. 25 and 26 and will be used in the following development.

If $f(x_i)$ is a quantity which depends on various system parameters, x_i, to each of which an elemental bias error, b_{x_i}, may be assigned, then the overall bias error, B_f, is defined by

$$B_f = \left[\sum_{i=1}^{N} \left(\frac{\partial f}{\partial x_i} \, b_{x_i} \right)^2 \right]^{1/2} \tag{21}$$

Similarly, an overall precision error, S_f, is related to the elemental precision errors, s_{x_i}, by

$$S_f = \left[\sum_{i=1}^{N} \left(\frac{\partial f}{\partial x_i} \, s_{x_i} \right)^2 \right]^{1/2} \tag{22}$$

The various elemental errors associated with a system are obtained from considerations related to the processes of 1) calibration, 2) signal processing and data acquisition, and 3) data reduction. The total uncertainty in the measurement obtained by the system is then (Refs. 25 and 26)

$$U_f = \pm \left(B_f - t_{0.95} \, S_f \right) \tag{23}$$

where $t_{0.95}$ is the 95th percentile point for the Student's t-distribution. For the degrees of freedom typical of an LDV data set, $t_{0.95} \approx 2.0$.

The LDV x-component velocity for the small angle approximation ($\sin \theta \approx \theta$) is given by

$$V_x = \frac{\lambda L}{DT} \tag{24}$$

where T is the period associated with the Doppler shift frequency, f_D, and L and D are defined in Fig. 12. The uncertainty in the wavelength, λ, is

$$\frac{\Delta\lambda}{\lambda} = \frac{\Delta\nu}{\nu + \Delta\nu} \approx 10^{-5} \tag{25}$$

where ν is the optical frequency corresponding to the 488.0- or 514.5-nm wavelength of the argon laser and is of the order $6(10^{14})$ Hz, and $\Delta\nu \approx 5(10^{9})$ Hz is the bandwidth of the laser gain profile. This uncertainty is insignificant and can be neglected. Bias errors for D and L were assumed to be zero since no significant bias error mechanism could be identified. Precision errors for D and L were determined by repeated measurements. For T values measured by the DDP instruments, the bias and precision error characteristics are signal-to-noise (S/N) ratio dependent. Reasonable estimates for the errors associated with T were obtained by laboratory experiments using simulated LDV signals with S/N characteristics similar to those observed with the LDV in Tunnel 4T. Table 2 lists the uncertainty parameters as determined under these conditions.

Substituting the values contained in Table 2 into Eqs. (21) through (23) shows that the uncertainty in V_x is

$$U_{V_x} = \pm \left(A_1 V_x^2 - A_2 V_x \sqrt{1 - A_3 V_x^2} \right) \tag{26}$$

where

$$A_1 = 7.32 \times 10^{-7} \text{ sec/ft}, \; A_2 = 1.03 \times 10^{-2}, \text{ and } A_3 = 3.25 \times 10^{-7} \text{ sec}^2/\text{ft}^2$$

Eq. (26) gives the uncertainty for a single velocity sample by the 4T LDV. The first term of Eq. (26)is caused by the S/N ratio-dependent bias error of the DDP instrument, whereas the $A_2 V_x$ term is predominantly attributable to the precision error associated with the determination of D. The final term, $A_3 V_x^2$, is indicative of the basic time resolution capability of the DDP (±0.01 nsec/LDV signal cycle) and the precision error induced in the measurements by S/N ratio effects.

The T precision error can be significantly reduced by exploiting time interval averaging (Refs. 16 and 19). Therefore, the uncertainty expression for mean velocity measurements, U_{V_x}, is the same as Eq. (26) except that the $A_3 V_x^2$ term approaches zero. Figure 16 is a plot of Eq. (26) versus measured velocity. It can be seen that the uncertainty in mean velocity measurements is close to ±1.1 percent of the measured value throughout the velocity range. The uncertainty in the single velocity samples starts at ±1.1 percent of the measured value at 500 ft/sec and increases to ±1.7 percent at 2,000 ft/sec. Those same T precision errors that average to zero for mean velocity measurements become bias errors for measurements of root mean square velocity deviation, V_x^*, about the mean velocity value. The interval between the two plots shown in Fig. 16 can be used to estimate the bias error for the V_x^* measurements.

Table 2. Uncertainty Parameters: Single-Velocity-Component Measurements

$\frac{\partial V_x}{\partial \lambda}$, 1/sec	b_λ, ft	s_λ, ft	$\frac{\partial V_x}{\partial L}$, 1/sec	b_L, ft	s_L, ft	$\frac{\partial V_x}{\partial D}$, -1/sec-	b_D, ft	s_D, ft	$\frac{\partial V_x}{\partial T}$, ft/sec^2	b_T, nsec	s_T, nsec
$\frac{V_x}{\lambda}$	0	0	$\frac{V_x}{L}$	0	0.02	$-\frac{V_x}{D}$	0	0.01	$-\frac{DV_x^2}{\lambda L}$	0.02	0.08
$2.7 \times 10^{-5} \times V_x$	0	0	$3 \times 10^{-2} \times V_x$	0	2×10^{-2}	$-5.1 \times 10^{-1} \times V_x$	0	1×10^{-2}	$3.66 \times 10^{4} \times V_x^2$	2×10^{-2}	8×10^{-2}

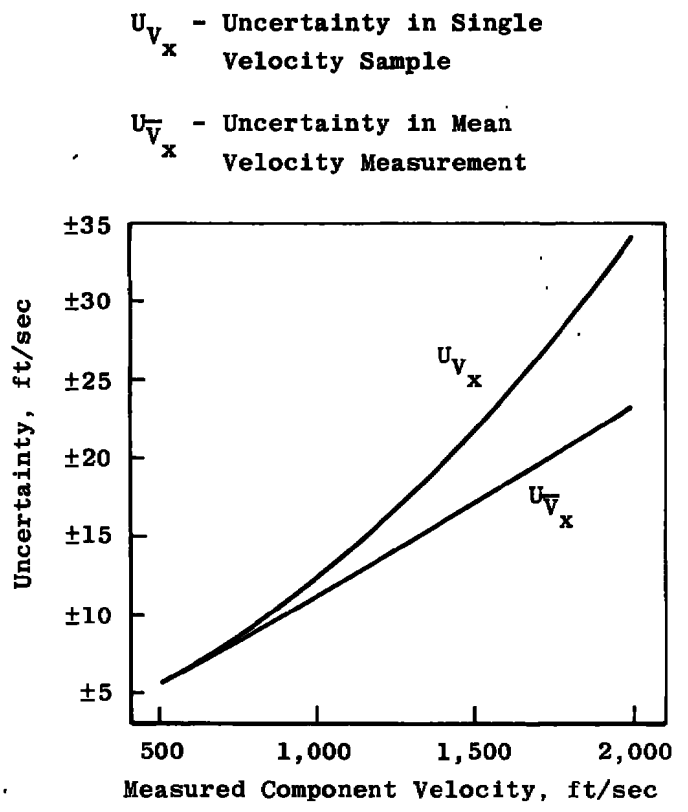

Figure 16. Uncertainty in the measurement of a single velocity component.

The expressions for the x-z plane velocity and flow angle as determined by the two-component LDV are given by Eqs. (15) and (16), respectively. It is seen that functional relations of the form

$$V = f(V_B, V_G, \gamma) \tag{27}$$

and

$$\phi = f(V_B, V_G, \alpha, \gamma, \Delta\alpha) \tag{28}$$

must be evaluated to obtain the elemental uncertainties associated with these measurements. Table 3 presents the coefficients, as well as bias and precision errors for V_{xz}, and Table 4 gives those for ϕ_{xz}. It is difficult to make a simple assessment of the overall uncertainty in the case of the two-component system since the coefficients associated with $U_{V_{xz}}$ and $U_{\phi_{xz}}$ are, themselves, functions of the individual variables. For example, the uncertainty associated with pitch plane velocity may be written as

$$U_V = \pm \left(A_1' V_B^2 + A_2' V_B \sqrt{1 + A_3' V_B^2} \right) \tag{29}$$

which is very similar to Eq. (26). The coefficients are, however, given by

$$A_1' = (7.32)\,(10^{-7})\ \frac{a}{c \sin\gamma}\sqrt{1 + \left(\frac{b}{a}\right)^2 \left(\frac{V_G}{V_B}\right)^4} \quad \text{(sec/ft)}$$

$$A_2' = (5.28)\,(10^{-5})\ \frac{a}{c \sin\gamma}\sqrt{1 + \left(\frac{b}{a}\right)^2 \left(\frac{V_G}{V_B}\right)^2 \left(\frac{1 + A_3 V_G^2}{1 + A_3 V_B^2}\right)} \tag{30}$$

$$A_3' = (3.25)\,(10^{-7})\ \text{sec}^2/\text{ft}^2$$

where

$$a = V_B - V_G \cos\gamma$$

$$b = V_G - V_B \cos\gamma \tag{31}$$

$$c = \left(V_G^2 - 2V_G V_B \cos\gamma - V_B^2\right)^{1/2}$$

The situation is even more complex for U_ϕ since the number of terms is greater. Consequently, it is preferable to use Eqs. (15), (16), (21), (22), and (23), Tables 3 and 4, and a specific set of data to compute the measurement uncertainties associated with V and ϕ. This is done for the data presentations of Section 5.0.

Table 3. Uncertainty Parameters: Two-Velocity-Component Measurements

$$\frac{\partial V_{xz}}{\partial V_B} = \frac{V_B - V_G \cos\gamma}{\sin\gamma\,(V_G^2 - 2V_B V_G \cos\gamma + V_B^2)^{1/2}}$$

$$b_{V_B} = (7.32 \times 10^{-7})\ V_B^2$$

$$s_{V_B} = \left[(2.64 \times 10^{-5})\ V_B^2 + (8.57 \times 10^{-12})\ V_B^4\right]^{1/2}$$

$$\frac{\partial V_{xz}}{\partial V_G} = \frac{V_G - V_B \cos\gamma}{\sin\gamma\,(V_G^2 - 2V_B V_G \cos\gamma + V_B^2)^{1/2}}$$

Table 3. Concluded

$$b_{V_G} = (7.32 \times 10^{-7})\ V_G^2$$

$$s_{V_G} = \left[(2.64 \times 10^{-5})\ V_G^2 + (8.57 \times 10^{-12})\ V_G^4\right]^{\frac{1}{2}}$$

$$\frac{\partial V_{XZ}}{\partial \gamma} = \frac{(V_G - V_B \cos\gamma)\ (V_B - V_G \cos\gamma)}{\sin^2\gamma\ (V_G^2 - 2V_BV_G \cos\gamma + V_B^2)^{\frac{1}{2}}}$$

$$b_\gamma = 0.0$$

$$s_\gamma = 0.14 \text{ deg}, \ \gamma = 89.1 \text{ deg}$$

Table 4. Uncertainty Parameters: Flow Angle Measurements

$$\frac{\partial \phi_{XZ}}{\partial V_B} = \frac{\sin\gamma\ (V_BV_G - V_G^2 \cos\gamma)}{(V_G^2 - 2V_BV_G \cos\gamma + V_B^2)\left[V_G^2\ (1 - \sin^2\gamma) - 2V_BV_G \cos\gamma + V_B^2\right]^{\frac{1}{2}}}$$

$$b_{V_B} = (7.32 \times 10^{-7})\ V_B^2$$

$$s_{V_B} = \left[(2.64 \times 10^{-5})\ V_B^2 + (8.57 \times 10^{-12})\ V_B^4\right]^{\frac{1}{2}}$$

$$\frac{\partial \phi_{XZ}}{\partial V_G} = \frac{\sin\gamma\ (V_BV_G \cos\gamma - V_B^2}{(V_G^2 - 2V_BV_G \cos\gamma + V_B^2)\left[V_G^2\ (1 - \sin^2\gamma) - 2V_BV_G \cos\gamma + V_B^2\right]^{\frac{1}{2}}}$$

$$b_{V_G} = (7.32 \times 10^{-7})\ V_B^2$$

$$s_{V_G} = \left[(2.64 \times 10^{-5})\ V_G^2 + (8.57 \times 10^{-12})\ V_G^4\right]^{\frac{1}{2}}$$

$$\frac{\partial \phi_{XZ}}{\partial \alpha} = 1$$

$$b_\alpha = 0.0$$

$$s_\alpha = 0.1 \text{ deg}$$

$$\frac{\partial \phi_{XZ}}{\partial_{\Delta\alpha}} = 1$$

Table 4. Concluded

$$b_{\Delta\alpha} = 0.0$$

$$s_{\Delta\alpha} = 0.002 \text{ deg}$$

$$\frac{\partial \phi_{XZ}}{\partial \gamma} = \frac{V_G \cos\gamma \,(V_G^2 - 2V_BV_G \cos\gamma + V_B^2) - V_BV_G^2 \sin^2\gamma}{(V_G^2 - 2V_BV_G \cos\gamma + V_B^2)\left[V_G(1 - \sin^2\gamma) - 2V_BV_G \cos\gamma + V_B^2\right]^{\frac{1}{2}}}$$

$$b_\gamma = 0.0$$

$$s_\gamma = 0.14 \text{ deg}, \ \gamma = 89.1 \text{ deg}$$

5.0 TEST RESULTS

5.1 SINGLE-VELOCITY-COMPONENT MEASUREMENTS

The single-velocity-component LDV system was used to evaluate (1) LDV performance using only intrinsic tunnel particulate matter as light scatterers and (2) the newly developed Doppler Data Analyzer (DDA).

5.1.1 LDV Signal Characteristics

As discussed in Section 2.2, the intrinsic sources of light-scattering particles in 4T are primarily dust-like particles and/or H_2O condensate. Light-scattering particles with diameters of the order of one micron or larger are required for proper operation of the present 4T LDV system when a conventional counter-type signal processor is used. Velocity information can be acquired from somewhat smaller particles by using specialized electronic signal processing instruments such as the DDA or instruments utilizing photon time-of-arrival correlation principles (Ref. 27).

A qualitative representation of the dependence of LDV time function signal characteristics upon particle size and number density is furnished in Fig. 17. Figure 17a shows a classical LDV signal waveform produced by a single particle (n = 1), with diameter d_a, passing through the LDV probe volume. Since a large number of photons are scattered by such a relatively large particle as it traverses the bright fringe planes, the resultant photodetected signal is well defined. However, as particle size decreases (Figs. 17b through e), the signals become less well defined, and discrete photon-detected events begin to be observed. Finally (Fig. 17e), the particle size is so small that only single photon-detected events mark the passage of the particle through the probe volume.

d - Particle Diameter
n - Number of Particles in the Probe Volume

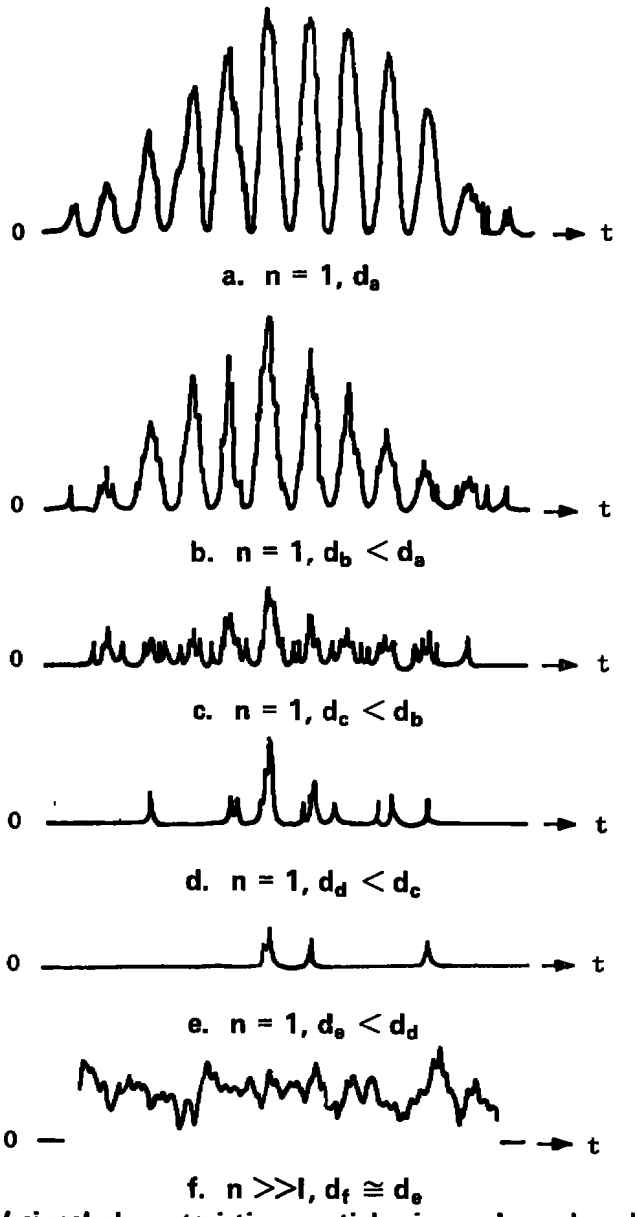

Figure 17. LDV signal characteristics: particle size and number density effects.

Figure 17f illustrates the situation wherein a large number (N>>1) of very small particles are simultaneously present in the probe volume. The resultant signal is chaotic and exhibits a power spectrum similar to that of a Guassian noise process.

The standard LDV signal processing instrument used at AEDC is the burst counter described in Section 3.4. This DDP can successfully be applied for signal types a through

c but fails, by design, when subjected to signal types d through f. The DDA instrument (Section 3.4) is usable for signal types a through e but fails for signal type f. The photon time-of-arrival correlation-type instrument could be used for signal types d through e but would also fail for signal type f. Useful velocity information from signal type f can be obtained only by direct optical detection of the Doppler shift frequency.

Qualitative, visual observations of oscilloscope displays of photodetector signals showed that signal type a was relatively rare in 4T, appearing about once every 15 to 20 seconds at Mach Number 0.8. For dry tunnel operating conditions (no H_2O condensate), most of the observed signals were of types d and e and occurred at a rate of about 10 to 50 per second at Mach Number 0.8. LDV operations were generally unsatisfactory under dry tunnel conditions at all Mach numbers because of the lack of adequate size particles. Photon correlation techniques were not evaluated because the LDV signal frequencies, for the velocity range encountered in 4T, were above the operating range of available instruments.

When condensate was formed over the Mach number range from 0.6 to 1.2, signals such as those shown in Fig. 17b were observed, and accurate LDV data could be routinely acquired. As tunnel operating conditions were varied to achieve Mach Number 1.3 operation, a distinct degradation in signal quality from type b to type c could be observed. This indicated some fundamental change in the condensation process. It is important to point out that only moderate levels of condensate are required for LDV operations and that excellent quality LDV signals derived from condensate have been observed in 4T although 1) the humidity level was within the specified limits for proper tunnel operation and 2) no condensate could be visually detected by the test section television cameras. In short, an LDV system is a very sensitive condensate detector. With moderate levels of condensation, LDV signal burst rates as high as 500,000 per second were observed and LDV velocity samples in excess of 1,000 per second were recorded using the DDP instrument.

When condensate was formed at Mach Numbers 1.6 and 2.0, scattered light levels great enough to saturate the photodetector were observed. This situation was caused by the high number density of small condensate particles formed at Mach numbers greater than about 1.3. The resulting signals looked like Fig. 17f and were useless for LDV purposes even after the photodetector was brought out of saturation. The signal waveform shown in Fig. 18 was recorded at Mach Number 1.6 by the high frequency waveform recorder. The initial portion of this recording shows a well-defined signal generated by a large particle. The remainder of the signal waveform was generated by a random-phased superposition of a large number of individual signals such as shown in Fig. 17e, produced by small condensate particles.

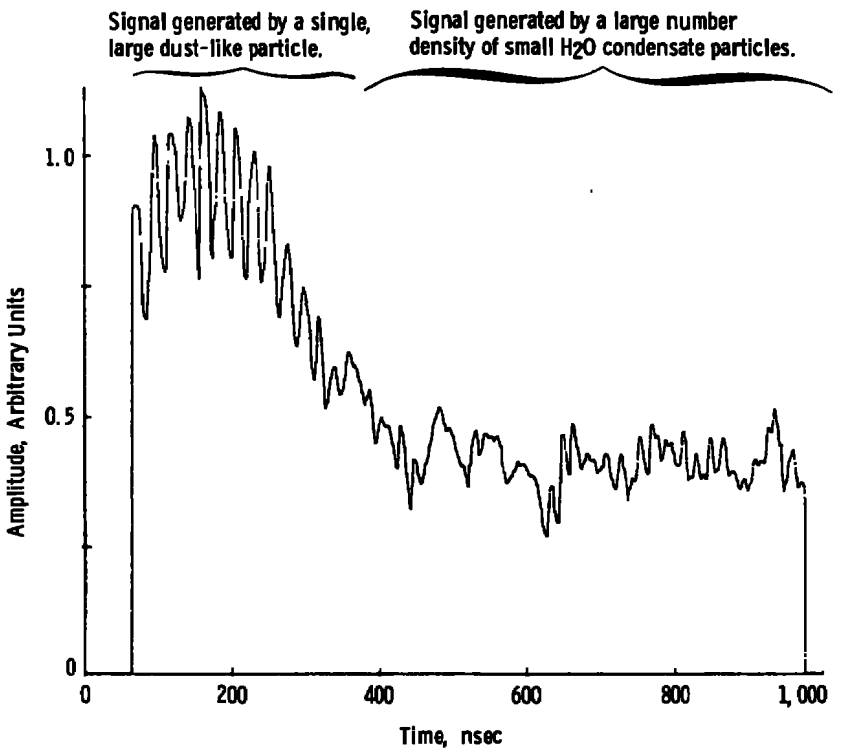

Figure 18. Signal waveform at Mach Number 1.6 with H_2O condensate.

A figure-of-merit is helpful in evaluating the usefulness of an LDV system installed in a certain aerodynamic test facility. To this end, LDV data productivity is here defined as the time required to record 1,000 individual velocity samples. Table 5 summarizes the LDV data productivity observed in Tunnel 4T. Clearly, the LDV is not satisfactory for routine data acquisition under most tunnel operating conditions since the time required to obtain a data set is generally too long. It is important to note that tunnel operation over the Mach number range from 0.6 to 1.3 accounts for about 90 percent of all testing in 4T. The present study suggests, therefore, that if humidity levels and/or thermodynamic conditions could be controlled to exploit condensate formation as a natural seeding mechanism, LDV operations over this Mach number range would be practical. Use of artificial seeding techniques, moreover, could substantially enhance the LDV data productivity at all Mach numbers. It is anticipated that future development and use of low-level LDV signal processors will result in at least moderate enhancement of LDV data productivity when only intrinsic particulate matter is available.

5.1.2 Tunnel Test Data

The single-velocity-component system was used to measure the axial, or x-axis, velocity component at a single y-axis position near the tunnel centerline.

Figure 19 shows mean velocity and estimated turbulence intensity data for the Mach number range from 0.6 to 1.2. LDV mean velocity measurements were compared to U_∞, the free-stream velocity derived from tunnel calibration procedures. Data points denoted by the circles were obtained from 1,000 DDP velocity samples, and the triangles represent data derived from 30,000 to 75,000 DDA velocity samples. The LDV mean velocity data are seen to compare with U_∞ to within 1.5 percent for the entire Mach number range shown and indicate a relative turbulence intensity of about 1.0 percent. This data comparison is affected, to some degree, by the fact that the LDV is essentially a point measurement device whereas U_∞ is a gross average quantity. Available, unpublished pitot-static probe data show similar velocity variations around U_∞. Therefore, some of the differences between $\overline{V}_x$ and U_∞ are attributable to local velocity deviations from U_∞.

Table 5. 4T LDV Data Productivity Summary

Conditions	Observed LDV Data Productivity[a]	Explanation
Mach Nos. 0.2 to 0.5	10 to 30 min	Low Number Density of Adequate Size Particulate Matter
Mach Nos. 0.6 to 1.3 Without H_2O Condensate	200 hr	Low Number Density of Adequate Size Particulate Matter
With H_2O Condensate	1 to 45 sec	Condensate Size and Number Density Ideal for LDV Operations
Mach Nos. 1.6 and 2.0 Without H_2O Condensate	200 hr	Low Number Density of Adequate Size Particulate Matter
With H_2O Condensate	>200 hr	Condensate Size Too Small and Number Density Too Large – LDV Signal is Large Amplitude But Chaotic

[a]Time required per 1,000 velocity samples with DDP signal processor

The number of LDV data points taken at each Mach number was determined by the length of time that the tunnel was held at that particular condition. Variations between data points at any one Mach number are caused by flow variations within the ±0.005 tolerance on tunnel Mach number setting and/or mean stagnation temperature changes with time.

Figure 19 also shows consistent agreement of the DDA mean velocity data compared to the DDP data. Further observations during this testing period showed that the DDA met its major design objective of being able to acquire data from small particulate matter. This was evidenced by the fact that the DDA was able to acquire accurate velocity data even after the DDP had ceased to function because of insufficient signal cycles. Even under good signal conditions the DDA data acquisition rate was about 5 to 1 greater than the DDP rate.

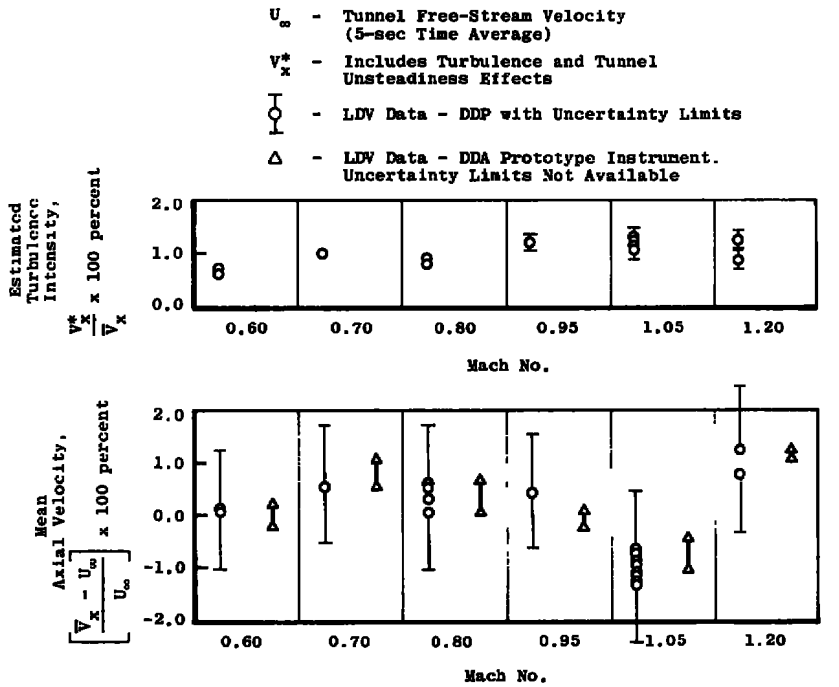

Figure 19. Single-velocity-component measurements at the tunnel centerline.

5.2 TWO-VELOCITY-COMPONENT AND FLOW ANGLE MEASUREMENTS

Figure 20 shows the apparatus details of a flow angularity survey recently conducted in Tunnel 4T. The rectangular x, y, z Cartesian coordinate system serves as a reference for the tunnel test section. The x-axis is coincident with the geometric tunnel centerline, and the y-z plane is located at the juncture of the expansion nozzle and test section. The aerodynamic flow angle probe was traversable in three dimensions, whereas the LDV probe volume was traversable only in the y-axis direction. The two-color LDV system shown in Fig. 7 was used to acquire x-z plane flow angle and velocity magnitude measurements for comparison with the aerodynamic flow angle probe measurements.

At its closest point of approach along the x-axis, the flow angle probe was still 9 in. downstream of the LDV probe volume scan axis. Most of the LDV data were recorded when the flow angle probe was 21 in. downstream at x = 108. Because of this x-axis separation, an obvious question is raised as to the significance of comparing flow angle probe and LDV data. The data shown in Fig. 21 were acquired to answer this question. From the three flow angle probe plots it is seen that 4T y-axis flow angle profiles are not a strong function of x-axis position at Mach number 0.8. This general characteristic is observed at all Mach numbers. Indeed, a maximum flow angle difference of only about 0.12 deg is observed for an x-axis separation as great as 24 in. Therefore, it is concluded that comparisons of LDV and flow angle probe data within about ±0.2 deg are meaningful. On this basis the LDV data are seen to compare quite favorably with the flow angle probe data.

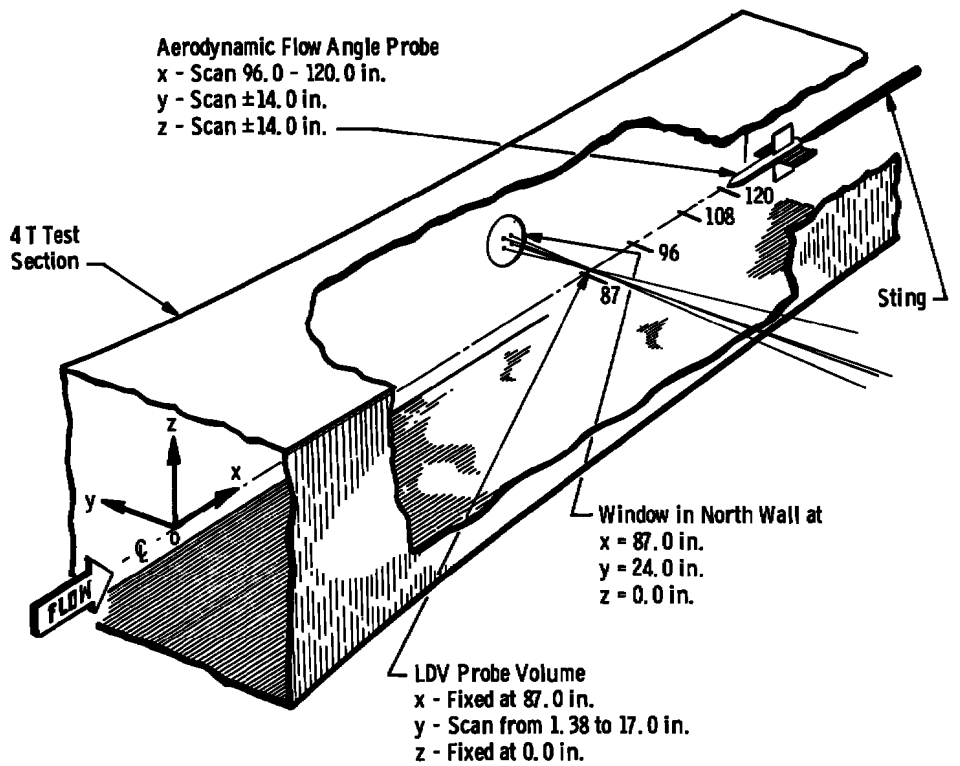

Figure 20. Apparatus details: flow angularity survey in Tunnel 4T.

To develop confidence in the two-velocity-component LDV measurements an experiment was conducted to relate LDV measurement repeatability to 1) tunnel unsteadiness and 2) particle lag effects. For the tunnel unsteadiness study the LDV system optical and electronic adjustments were optimized and then not touched until five consecutive data points had been recorded. The nominal tunnel operating conditions were constant throughout this experiment. These data are shown in Fig. 22. The extremes in flow angle are seen to differ by 0.07 deg. The extremes in the mean velocity magnitude measurements are seen to differ by 0.25 percent. The expected statistical variability in the LDV mean velocity data is given by the formula for the standard deviation of mean values for sets of N measurements (Ref. 28):

$$\frac{s_{\bar{V}}}{\bar{V}} = \frac{1}{\sqrt{N}} \left(\frac{V^*}{\bar{V}}\right) \tag{32}$$

For $V^*/\bar{V} \approx 1.5$ percent (experimental determination) and N = 750 (see Fig. 22), $s_{\bar{V}}/\bar{V}$ equals approximately 0.05 percent. Since the statistical variability was less than the observed variability, it was concluded that DDP signal processor stability and tunnel unsteadiness were primarily responsible for the velocity data variability. The same conclusion was reached concerning the variability in flow angle data.

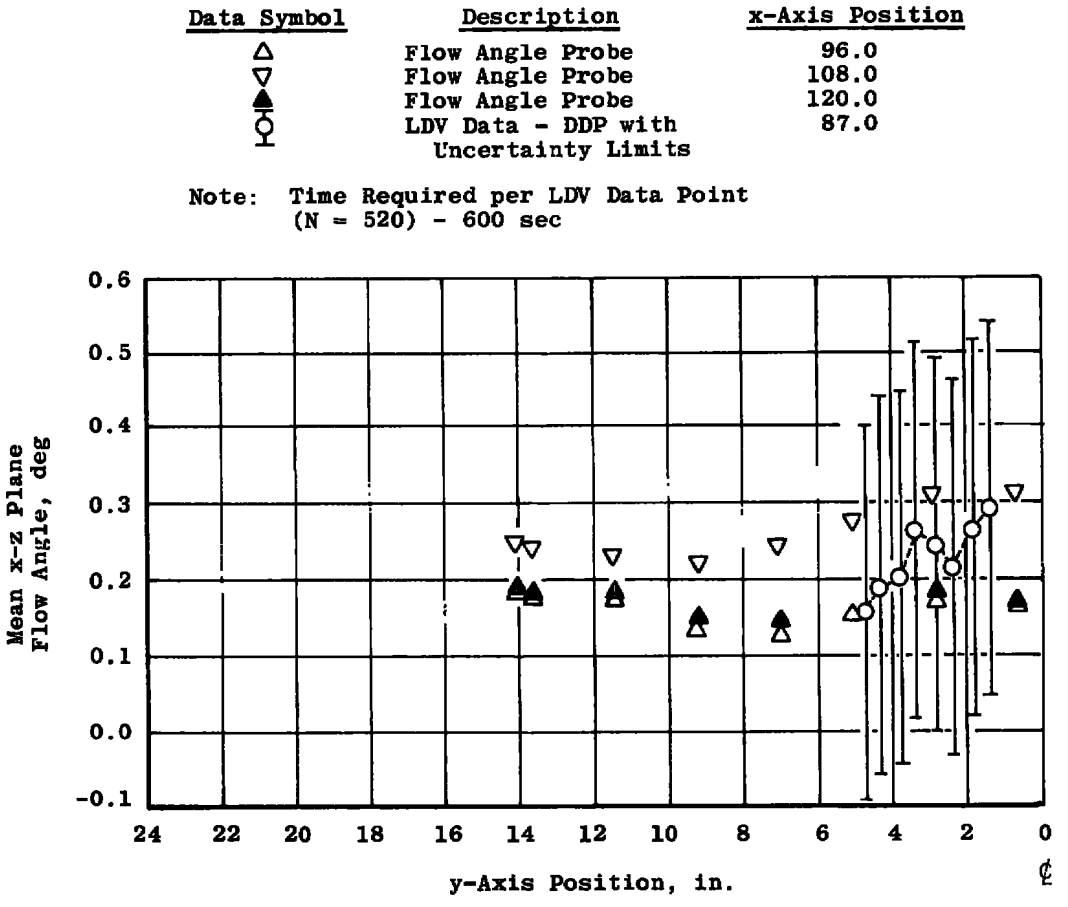

Figure 21. Sensitivity of x-z plane flow angle to x-axis position at Mach number 0.8.

The particle lag experiment was conducted immediately following the tunnel unsteadiness study. The nominal tunnel operating conditions were again held constant throughout the time LDV data were being recorded. All LDV operating parameters were held constant except for the oscilloscope trigger level, which can be used as a signal amplitude discriminator. The trigger adjust was first set at a low level so that all signals produced by the LDV system were displayed by the oscilloscope and were thereby available to the DDP for production of velocity sample measurements. Under these conditions a large percentage of the LDV data are derived from small particles. As the trigger level is increased, the signals from the smaller particles are excluded. At the high trigger level setting, only signals generated by the largest particles in the flow are available for processing by the DDP instruments. If particle lag were a problem, then the mean velocity of the large particles would be expected to be lower than that of the smaller particles.

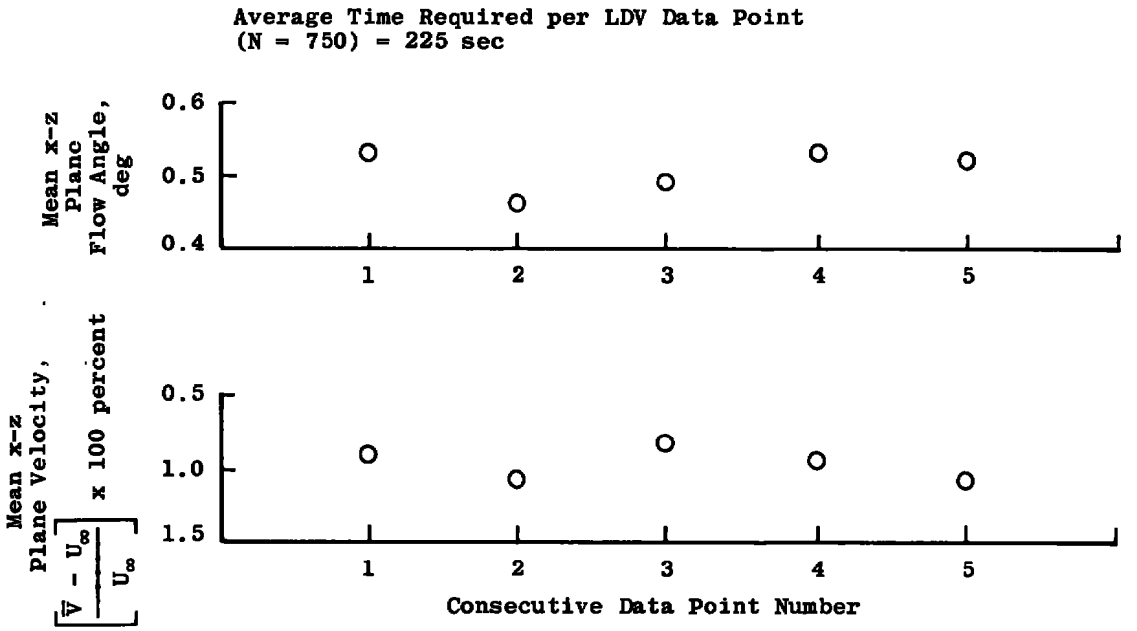

Figure 22. LDV measurement repeatability test at Mach Number 0.8.

Figure 23 shows the results of the particle lag experiment. The flow angle extremes are seen to differ by 0.12 deg, whereas the extremes in velocity magnitude differ by 0.2 percent. This data variability is comparable to that shown in Fig. 22, which was attributed to tunnel unsteadiness and DDP signal processor stability; thus there is no increase in data variability associated with particle lag effects. On the basis of this experiment, particle lag does not appear to be a significant problem for 4T free-stream mean velocity and flow angle measurements when intrinsic particulate matter is used.

Figure 24 compares LDV, aerodynamic flow angle probe data, and free-stream velocity data. The tunnel was operated at two slightly different diffuser flap positions during the time required to complete the LV y-axis scan; this variation caused the observed discontinuity in the flow angle data. The LDV flow angle profile is seen to compare with the flow angle probe data to within 0.2 deg, which is within the uncertainty limits of the LDV measurements. LDV velocity magnitudes compare with U_∞ within 1.3 percent at the four y-axis positions. This slightly exceeds the ±1.1 percent uncertainty limits for the LDV data but still represents good data agreement.

Figure 25 shows comparison data taken at Mach Number 0.4. Again, tunnel conditions were changed before the LDV y-axis scan could be completed. It is noted that in response to the tunnel condition change, the flow angle probe data show a "jump" of 0.37 deg compared to 0.30 deg for the LDV system. Before and after the jump the LDV

data compare with the flow angle probe data within 0.1 deg. For one set of tunnel conditions the LDV velocity was about 1.4 percent lower than U_∞, whereas for the second set of tunnel conditions the LDV velocity was about 1.4 percent greater than U_∞.

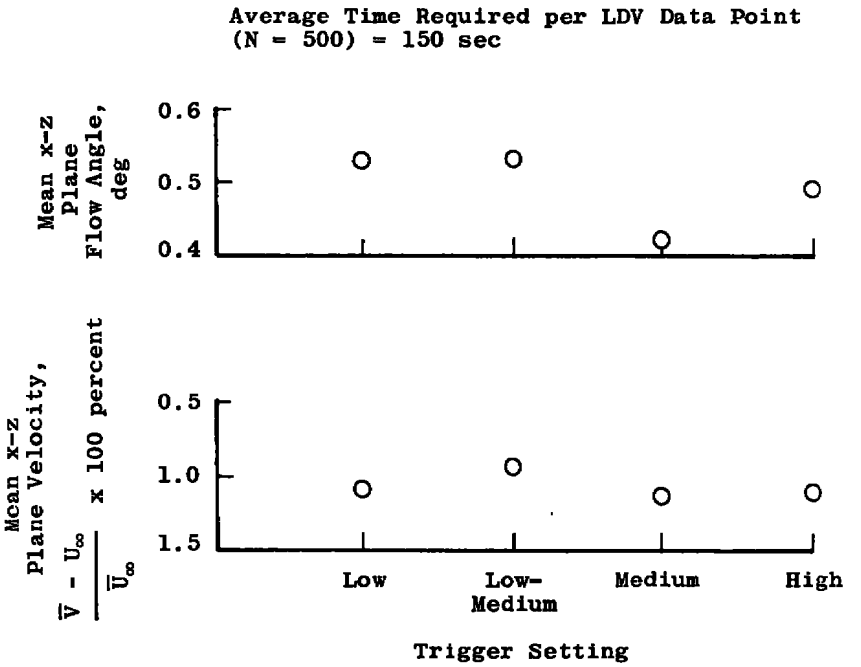

Figure 23. Effect of trigger setting (particle size) on LDV measurement repeatability at Mach number 0.8.

The data included in Figs. 24 and 25 were acquired using intrinsic particles as light scatterers, and the relatively long time period required for LDV data acquisition is noted. Figure 26 shows LDV data recorded at Mach number 0.8 with H_2O condensate purposely formed in the tunnel test section. These data were taken during a preliminary investigation in Tunnel 4T to determine whether H_2O condensate formation could be controlled and thereby exploited to provide particulate matter when required for LDV operations. The tunnel conditions were set at Mach number 0.8, total temperature 88.4°F, and stagnation pressure 2,000 lb/ft^2. During normal tunnel operation the tunnel circuit makeup air is passed through a desiccant material to remove the H_2O vapor and thereby suppress condensate formation. During this investigation, however, atmospheric makeup air was used. This resulted in condensate formation, excellent LDV signal characteristics, and data rates up to 200 velocity samples per second. Following the acquisition of the LDV data, only about 10 minutes were required to change over from the atmospheric makeup air source to the dry source. Under the dry conditions, LDV

operations were entirely unsatisfactory since a data rate of about one velocity sample per second was observed. No flow angle probe data were available for inclusion in Fig. 27, but the LDV velocity data are seen to compare with U_∞ within 0.8 percent for the entire y-axis profile.

Data Symbol	Description	x-Axis Position
△	Flow Angle Probe	108.0
⧋	U_∞ - Tunnel Free-Stream Velocity (5 sec Time Average)	---
⊥○⊥	LDV Data - DDP with Uncertainty Limits	87.0

Note: Time Required per LDV Data Point (N = 300) = 265 sec

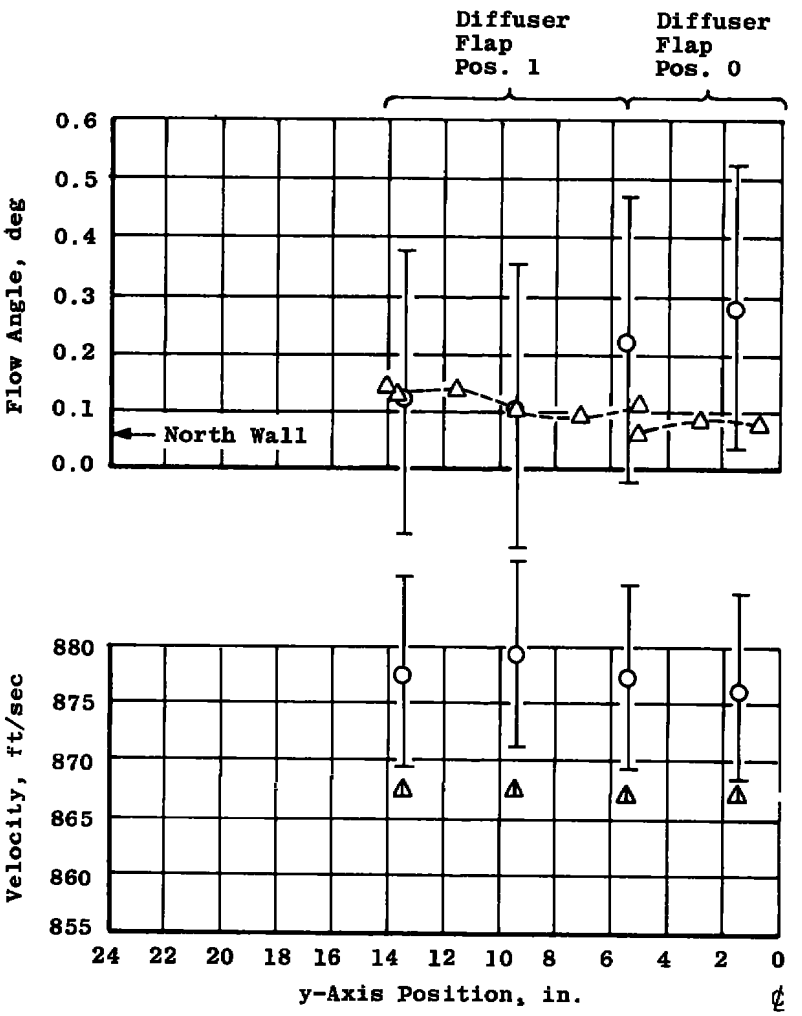

Figure 24. Scan of y-axis: x-z plane flow angle and velocity magnitude measurements at Mach Number 0.8.

Data Symbol	Description	x-Axis Position
△	Flow Angle Probe	108.0
⏃	U_∞ - Tunnel Free-Stream Velocity (5 sec Time Average)	---
⊖	LDV Data - DDP with Uncertainty Limits	87.0

Note: Time Required per LDV Data Point (N = 300) = 215 sec

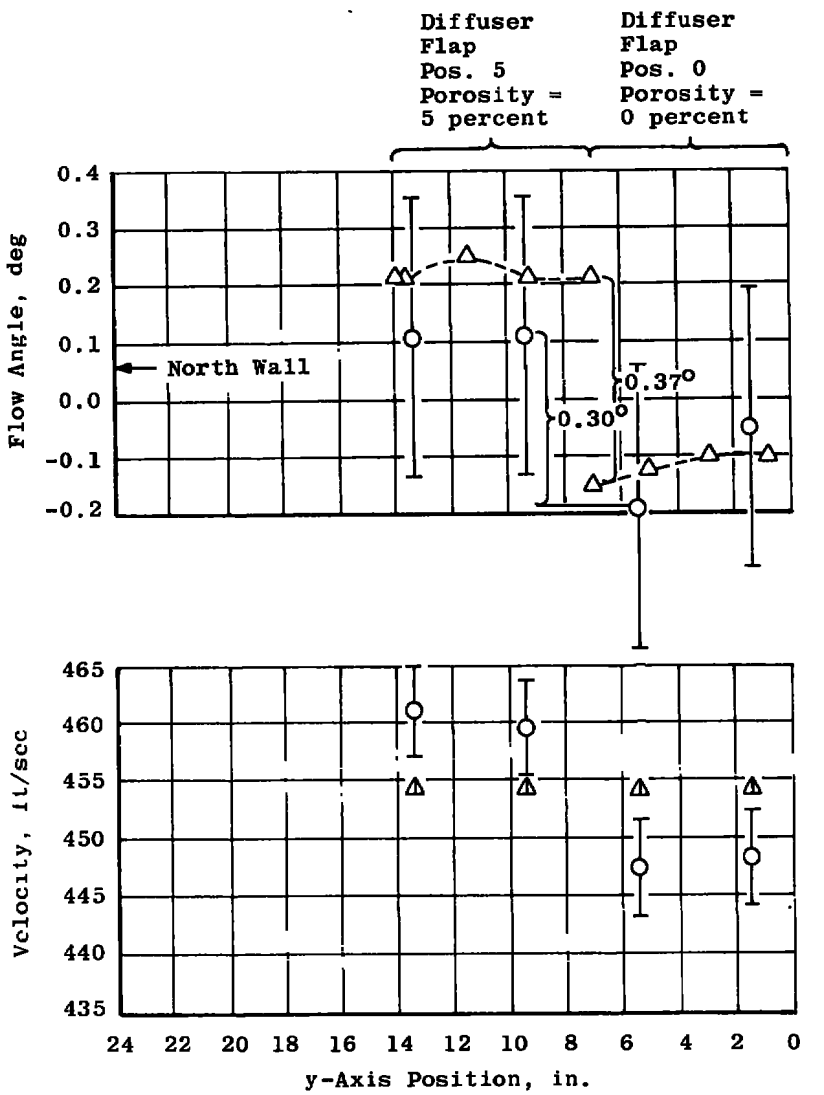

Figure 25. Scan of y-axis: x-z plane flow angle and velocity magnitude measurement at Mach number 0.4.

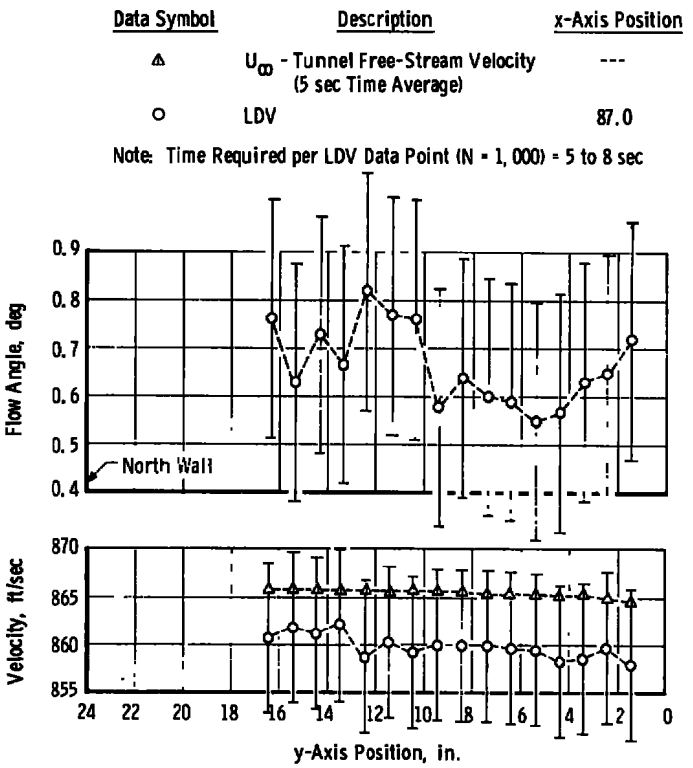

Figure 26. LDV data with H_2O condensate purposely formed at Mach number 0.8.

6.0 SUMMARY OF RESULTS AND CONCLUSIONS

A two-velocity-component LDV system was developed and operated in the AEDC-PWT 4-ft Transonic Wind Tunnel (4T) to determine the capabilities and limitations of LDV technology as adapted for application in a large aerodynamic test facility.

This study has shown that usefully accurate flow angle and velocity magnitude data can be obtained by LDV techniques in a large test facility such as 4T. However, exclusive reliance upon intrinsic particulate matter for light scatterers is a fundamental limitation on the data productivity of the LDV system. Without H_2O condensate, the LDV data rate in 4T was objectionably low at all Mach numbers because of the low number density of adequate size dust-like particles. With low levels of H_2O condensate, scatter particle characteristics (size and number density) were ideal for LDV operations over the Mach number range from 0.6 to 1.3. Above Mach Number 1.3 the condensate particle size was too small and number density too large for useful LDV measurements.

State-of-the-art, two-color LDV optics were developed for use in 4T. This represents the first use of such a system at AEDC. Unique, remotely controlled optical alignment techniques and devices were developed and successfully applied. An environmental

control system was developed to house the LDV optics and counter the detrimental effects of the 4T environmental factors. A new, low-level signal processor termed the Dopper Data Analyzer was developed and evaluated. A versatile, computer-controlled data acquisition system was also developed for the 4T LDV system. All systems performed satisfactorily.

A measurement uncertainty analysis of the 4T LDV system indicates that the uncertainty in mean x-z plane velocity magnitude is within ±1.1 percent of the measured value. The uncertainty in x-z plane flow angle measurements was found to be ±0.25 deg. The major portion of these uncertainties is attributable to the presently used LDV calibration techniques. Development of more precise calibration techniques is required for further reduction of measurement uncertainties.

The uncertainty in each individual velocity and flow angle measurement is greater than the associated mean value uncertainty and increases with velocity because of the finite time resolution capabilities of the LDV signal processor. Increased digital clock frequency and/or improved analog pulse stretcher stability is called for to reduce this uncertainty factor. Both improvement approaches are presently practical and merit further study.

The uncertainty in discrete velocity and flow angle measurements and associated root mean square values is a strong function of, and is directly related to, the ratio of noise signal magnitude to LDV signal magnitude. Mechanical constraints dictated the use of a coaxial backscatter-type LDV receiver in Tunnel 4T. For certain traverse positions of the LDV receiver, noise signals with amplitudes greater than the LDV signals were observed. The noise source in this case was transmitter laser light reflected and scattered off the wind tunnel window. The use of an off-axis backscatter receiver would have significantly reduced the stray laser light noise signal. Experience at 4T and other AEDC test facilities has shown that the off-axis backscatter receiver is the system of choice when one is confronted with test section windows.

The 1.5-percent comparison of LDV mean velocity magnitude measurements with U_∞ values was encouraging, as was the ±0.2-deg comparison of LDV and aerodynamic flow angle probe data. However, it should be emphasized that attainment of usefully accurate LDV data in a large aerodynamic test facility such as 4T can require expenditures of design and operations efforts at least an order of magnitude greater than simpler applications where such factors as tightly scheduled tunnel operations, hostile environment (vibration, vacuum, etc.), and remote and inacessible location of the LDV system are not encountered.

REFERENCES

1. Bentley, H. T. and Bomar, B. W. "Development of a Laser Velocimeter System for Flame Studies." AEDC-TR-76-150 (ADA041216), June 1977.

2. Lennert, A. E., Sowls, R. E., Belz, R. A., Goethert, W. H., Bentley, H. T., Powell, H. M., Bailey, A. B., and McKay, T. D. "Electro-Optical Techniques for Diesel Engine Research." AEDC-TR-77-17 (ADA039357), May 1977.

3. Alt, R. E., Frazine, D. F., and Brayton, D. B. "AFRPL Rocket Plume Measurements." AEDC-TR-76-95 (ADB014933L), November 1976.

4. Barnett, D. O. and Brayton, D. B. "Laser Velocimeter Utilization in Jet Engine Test Cells." AEDC-TR-77-21 (ADA041019), June 1977.

5. Weyer, H. B., Lecture Series Director. "Laser Optical Measurement Methods for Aero Engine Research and Development." AGARD Lecture Series No. 90, Trenton, New Jersey, July, 1977.

6. Cline, V. A. and Lo, C. F. "Application of the Dual Scatter Laser Velocimeter in Transonic Flow Research." AGARD Conference Proceedings No. 193 on Applications of Non-Intrusive Instrumentation in Fluid Flow Research, Saint-Louis, France, May 1976, pp. 4-1 to 4-12.

7. Lo, C. F. and Heltsley, F. L. "Interpretation of Laser Velocimeter Measurements in a Transonic Flow Field." Twenty-Second ISA Aerospace Instrumentation Symposium, San Diego, California, May 1976.

8. Kalb, H. T. and Cline, V. A. "New Technique in the Processing and Handling of Laser Velocimeter Burst Data." Review of Scientific Instruments, Vol. 47, No. 6, June 1976, pp. 708-711.

9. Hsieh, T. "Analysis of Velocity Measurements about a Hemisphere-Cylinder Using a Laser Velocimeter." Journal of Spacecraft and Rockets, Vol. 14, No. 5, May 1977, pp. 280-283.

10. Gunn, J. A. and Maxwell, H. "Calibration of the AEDC-PWT Aerodynamic Wind Tunnel (4T) Mach Numbers 1.6 and 2.0 Nozzle Blocks." AEDC-TR-72-111 (AD749513), September 1972.

11. Durst, F., Melling, A., and Whitelaw, J. H. Principles and Practice of Laser-Doppler Anemometry. Academic Press, New York, 1976.

12. Brayton, D. B., Kalb, H. T. and Crosswy, F. L. "Two-Component Dual-Scatter Laser Doppler Velocimeter with Frequency Burst Signal Readout." Applied Optics, Volume 12, No. 6, June 1973, pp. 1145-1156.

13. Crosswy, F. L. and Hornkohl, J. O. "Signal Conditioning Electronics for a Laser Vector Velocimeter." Review of Scientific Instruments, Vol. 44, No. 9, September 1973, pp. 1324-1332.

14. Farmer, W. M. and Hornkohl, J. O. "Two-Component, Self-Aligning Laser Vector Velocimeter." Applied Optics, Vol. 12, No. 11, November 1973, pp. 2636-2640.

15. Grant, G. R. and Orloff, K. L. "Two-Color Dual-Beam Backscatter Laser Doppler Velocimeter." Applied Optics, Vol. 12, No. 12, December 1973, pp. 2913-2916.

16. Barnett, D. O. and Giel, T. V. "Application of a Two-Component Bragg-Diffracted Laser Velocimeter to Turbulence Measurements in a Subsonic Jet." AEDC-TR-76-36 (ADA025355), May 1976.

17. Kalb, H. T., Brayton, D. B., and McClure, J. A. "Laser Velocimetry Data Processing." AEDC-TR-73-116 (AD766418), September 1973.

18. Cline, V. A. "A Laser Velocimeter for the AEDC Acoustic Research Tunnel." AEDC-TR-77-53 (ADA040903), June 1977.

19. Hewlett-Packard Application Note 162-1. "Time Interval Averaging."

20. Lennert, A. E., Brayton, D. B., Crosswy, F. L., Goethert, W. H., Kalb, H. T., and Smith, F. H. "Summary Report of the Development of a Laser Velocimeter to be Used in AEDC Wind Tunnels." AEDC-TR-70-101 (AD871321), July 1970.

21. Brayton, D. B. and Goethert, W. H. "A New Dual-Scatter Laser Doppler-Shift Velocity Measuring Technique." ISA Transactions, Vol. 10, No. 1, 1971, pp. 40-50.

22. Cebici, T. and Smith, A. M. O. Analysis of Turbulent Boundary Layers. Academic Press, New York, 1974.

23. Barnett, D. O. and Bentley, H. T. "Statistical Bias of Individual Realization Laser Velocimeters." Proceedings of the Second International Workshop on Laser Velocimetry, Engineering Experiment Station, Bulletin No. 144, Purdue University, West Lafayette, Indiana, March 1974.

24. McLaughlin, D. K. and Tiederman, W. G. "Biasing Correction for Individual Realization of Laser Anemometer Measurements in Turbulent Flows." Physics of Fluids, Vol. 16, No. 12, December 1973, pp. 2082-2088.

25. Abernethy, R. B., Colbert, D. L., and Powell, B. D. "ICRPG Handbook for Estimating the Uncertainty in Measurements Made with Liquid Propellant Rocket Engine Systems." CPIA No. 180, April 1969.

26. Abernethy, R. B. et al., Pratt and Whitney Aircraft, and Thompson, J. W., ARO, Inc. "Handbook-Uncertainty in Gas Turbine Measurements." AEDC-TR-73-5 (AD 755356), February 1973.

27. Mayo, W. T. Jr. "Digital Photon Correlation Data Processing Techniques." AEDC-TR-76-81 (ADA027195), July 1976.

28. Cooper, G. R. and McGillem, C. D. Probabilistic Methods of Signal and System Analysis. Holt, Rinehart, and Winston, New York, 1971.

NOMENCLATURE

A_1, A_2, A_3	Constant coefficients, Eq. (26)
A_1', A_2', A_3'	Variable coefficients, Eq. (29)
a,b,c	Variable coefficients, Eq. (30)
B	Overall system bias error, Eq. (21)
b_{x_i}	Elemental bias error, Eq. (21)
D	Distance between LDV transmitter beams, Fig. 12
$d_a, d_b, d_c, d_d, d_e, d_f$	Diameters of light-scattering particles, Fig. 18
$f(x_i)$	Generalized function of x_i variable, Eq. (21)
f_D	Doppler or LDV signal frequency, Eq. (3)
K_v	LDV calibration constant, Eq. (5)
$\vec{k}$	Propagation vector, Eq. (3)
L	Distance from LDV probe volume, Fig. 12
M	Number of histograms, Eq. (2)
N	Number of discrete samples, Eqs. (1), (8), (9), and (32)
n	Number of light-scattering particles in the probe volume, Fig. 18
P	Number of cycles counted by the LDV signal processor, Eq. (1)
S	Overall measurement system precision error, Eq. (22)
$s_{\overline{V}}$	Standard deviation of $\overline{V}$ values
s_{x_i}	Elemental precision error, Eq. (22)
T	LDV signal period, Eqs. (1) and (24)
$t_{0.95}$	95th percentile point for the two-tailed Student's "t" distribution, Eq. (23)
U	Total measurement system uncertainty, Eq. (23)

U_∞	Tunnel free-stream velocity, Figs. 19, 22, and 23
$\overline{u}$	Mean value of u, Eq. (8)
u'	Instantaneous deviation of u from $\overline{u}$, Eq. (7)
u^*	Root mean square deviation of u from $\overline{u}$, Eq. (9)
$u_\perp$	Unit vector normal to the LDV fringe planes, Eq. (4)
u, v, w	Instantaneous velocity components in the x, y, and z directions, respectively, Section 4.2
V	x-z plane velocity magnitude measurement, Eq. (15)
$\overline{V}$	Mean of V values, Eq. (19)
$\vec{V}$	x-z plane velocity vector, Fig. 15
V_x	Velocity component measurement in the x direction, Eq. (12)
$\overline{V}_x$	Mean of V_x values, Eq. (12)
V_x^*	Root mean square variation of V_x values about $\overline{V}_x$
x,y,z	Rectangular, Cartesian coordinate axes
α	Angle subtended by the green fringe planes and the z-coordinate axis, Fig. 14
β	Angle subtended by the blue fringe planes and the z-coordinate axis, Fig. 14
γ	Sum of angles α and β, Fig. 15
$\Delta\lambda$	Small uncertainty in the value of λ, Eq. (25)
θ	Angle subtended by the LDV transmitter beams, Eq. (4)
λ	Laser wavelength, Eq. (25)
ν	Optical frequency, Eq. (25)
σ	Relative turbulence intensity, Eq. (10)

$\hat{\sigma}$	Estimate of σ derived from LDV measurements, Eq. (13)
ϕ	Flow angle

SUBSCRIPTS

B	Blue
G	Green
f	General function
i	Index for a discrete event or quantity
j	Index for LDV histogram data, Eq. (1)
xz	Denotes x-z plane

ABBREVIATIONS

ASCII	American Standard Code for Information Interchange
CPU	Central processing unit, Fig. (11)
CRT	Cathode ray tube
DAS	Data acquisition system
DDA	Doppler data analyzer
DDP	Doppler data processor
ECS	Environmental control system
LDV	Laser Doppler Velocimeter
PMT	Photomultiplier tube
PWT	Propulsion Wind Tunnel
rms	Root mean square